Synthesis of novel biocomposite powder for simultaneous removal of hazardous ciprofloxacin and methylene blue: Central composite design, kinetic and isotherm studies using Brouers-Sotolongo family models

Sarra KAROUI[1,2,3], Rim BEN ARFI[1], Karine MOUGIN[4], Achraf GHORBAL[1,5] Aymen ASSADI[3], Abdeltif AMRANE[3]

[1] Research Laboratory LR18ES33, National Engineering School of Gabes, University of Gabes, Tunisia

[2] National Engineering School of Sfax, University of Sfax, Tunisia

[3] Univ Rennes, École Nationale Supérieure de Chimie de Rennes, CNRS, ISCR (Institut des Sciences Chimiques de Rennes) – UMR 6226, F-35000 Rennes, France

[4] Institute of Materials Science of Mulhouse, CNRS - UMR 7361, University of Haute-Alsace, France

[5] Higher Institute of Applied Sciences and Technology of Gabes, University of Gabes, Tunisia

Graphical Abstract

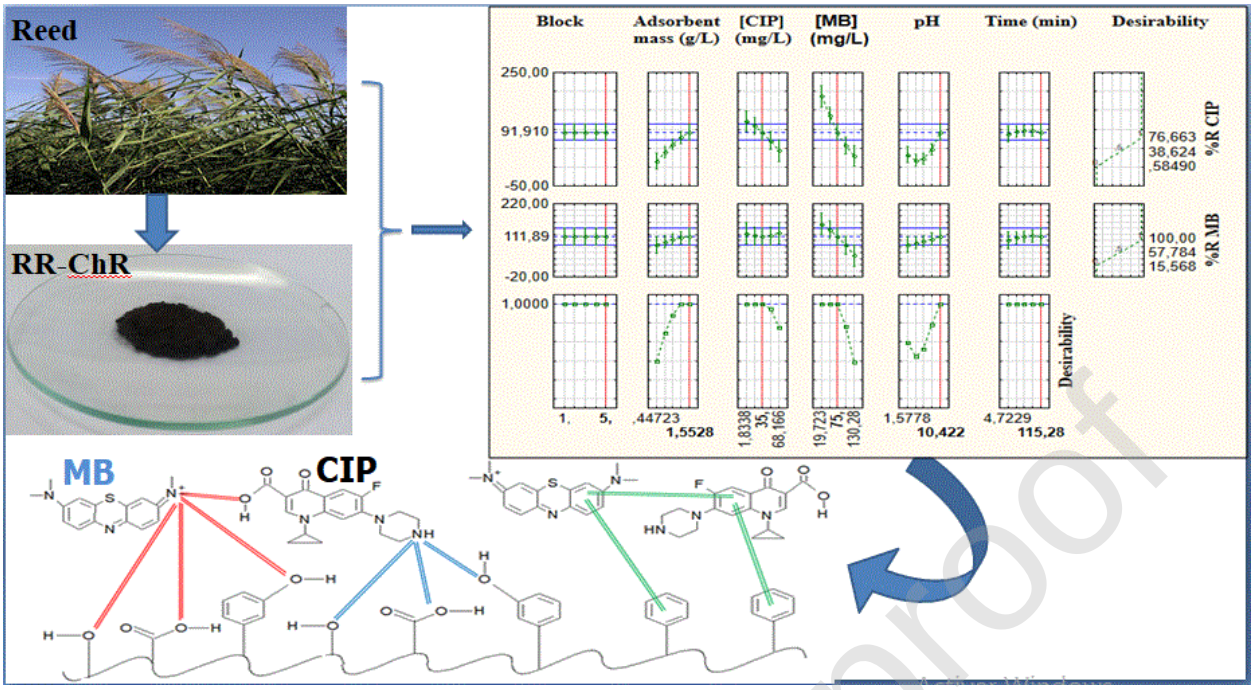

Highlights

- Novel biocomposite powder was simply prepared from Reed plant.
- Ciprofloxacin and methylene blue were first time simultaneously removed.
- Operating parameters were optimized by CCD-RSM methodology.
- Kinetic and isotherm models were studied using Brouers-Sotolongo family equations.
- Biosorption mechanisms were discussed.

Abstract

Over the past decades, extensive efforts have been made to use biomass-based-materials for wastewater-treatment. The first purpose of this study was to develop and characterize regenerated-reed/reed-charcoal (RR-ChR), an enhanced biosorbent from Tunisian-reed (*Phragmites-australis*). The second aim was to assess and optimize the RR-ChR use for the removal of binary ciprofloxacin antibiotic (CIP) and methylene blue dye (MB), using Central Composite Design under Response Surface methodology. The third purpose was to explain the mechanisms involved in the biosorption-process. The study revealed that the highest removal-percentages (76.66% for the CIP and 100% for the MB) were obtained under optimum conditions: 1.55 g/L of adsorbent, 35 mg/L of CIP, 75 mg/L of MB, a pH of 10.42 and 115.28 min contact time. It showed that the CIP biosorption mechanism was described by Brouers–Sotolongo-fractal model, with regression-coefficient (R^2) of 0.9994 and a Person's Chi-square (X^2) of 0.01. The Hill kinetic model better described the MB biosorption (R^2=1 and X^2=1.0E-4). The isotherm studies showed that the adsorbent surface was heterogeneous and the best nonlinear-fit was obtained with the Jovanovich (R^2=0.9711), and Brouers–Sotolongo (R^2=0.9723) models, for the CIP and MB adsorption, respectively. Finally, the RR-ChR lignocellulosic-biocomposite-powder could be adopted as efficient and cost-effective adsorbent.

Keywords: Biocomposite material; Pollutants removal; Central composite design; Kinetics; Isotherms.

Introduction

Dyes are widely used in many sectors such as cosmetic products, print shops, food, and clinical products, and especially in textile industries. The world production of dyes is estimated at more than 800,000 tons per year [1]. Indeed, approximately 15% of the total dyestuff is lost during the dyeing process in different textile industries and comes out with their wastewater [2]. Methylene Blue (MB) is one of the most used dyes for several applications such as coloring paper, wool and cotton. In addition to dyestuff, considerable amounts of antibiotics are discharged by pharmaceutical industries causing serious aquatic pollution. This latter pollutant was also reported to be discharged into the environment as unmetabolized parent compounds directly within urine and feces [3]. In particular, one of the common antibacterial molecules, the ciprofloxacin (CIP), used for clinical medical treatments [4] was detected in surface water, ground water, wastewater, sewage, soils and sediments [5]. Moreover, antibiotics and dyes, as organic wastes, are frequently encountered together in the wastewaters of lakes, for instance [6]. Because of their stability, their low biodegradability, their carcinogenic and mutagenic nature, dyes and antibiotics present a real danger to humans and their environment [7]. Above all, CIP and MB often coexist in wastewater and soils. For this reason, different types of biological and physico-chemical methods were tested to remove them. Instances of these are coagulation-flocculation, membrane filtration [8,9], chemical oxidation [10,11], photocatalytic degradation [12], electrochemical degradation [13], sonocatalytic degradation [14], ion exchange [15], electrochemical methods and adsorption [16]. Therefore, there was a wealth of research on the simultaneous removal of various kinds of pollutants such as, dye-dye [17,18], antibiotic-antibiotic [19,20], heavy metal-heavy metal [21], dye-heavy metal [22,23] and antibiotic-heavy metal [24,25].

However, despite the common presence of antibiotics and dyes in industrial wastewaters, there is a dearth of studies investigating their simultaneous binary removal and most works focused on the removal of one pollutant at a time. This paper is the first comprehensive study that has evaluated the simultaneous removal of CIP, as antibiotic, and MB, as dye, from water. In addition, although adsorption is considered as the favorite process to treat wastewater because of its simplicity, high efficiency, rapidity, eco-friendliness [26] and cost effectiveness [27]. Additionally, researchers have considered various conventional adsorbents such as silica- multiwall carbon nanotubes, silica/carbon nanotubes and silica/activated carbon [28–30], biomaterials [31,32], and other adsorbents have been investigated for various

pollutants removal but they are not highly efficient. However, it seems that research has not yet succeeded to produce the most efficient adsorbent to remove two pollutants at the same time. Therefore, research studies are still making great efforts to synthesize new biosorbents with high capacities and efficacies for binary pollutants removal. Therefore, this work purported a three- fold objective. Firstly, it intended to conduct a comprehensive investigation of the possibility to synthesize a novel, cost effective and environment friendly bio-composite powder extracted from Tunisian reed (Phragmites australis) and used as a biosorbent. The Tunisian reed is an invasive plant that flourishes extensively in marshes in the Gabes region (Tunisia) and causes an environmental problem. Secondly, it intended to assess the capability and efficiency of this novel adsorbent to remove antibiotics and dyes from water simultaneously. Thirdly, this work would rid the environment of dyes, antibiotics and the invasive plants. All this requires simple processing methods and little expenses compared to other adsorbents extracted from costly materials.

The designs are more advantageous than traditional single parameter testing approaches, because they enable the modeling and the optimization of multiple variables with a strongly reduced number of experiments. On top of that, The Box-Behnken Design (BBD) and Central Composite Design (CCD), as RSM techniques, are the most efficient to accurately analyze the relationship between variables and the effect of individual variables [33]. Compared to the CCD, the BBD procedure does not include extreme factor value combinations (highest or lowest level) [34]. Therefore, the CCD can perform runs under extreme factor value conditions, ensuring accurate results. The fourth goal of this work was to assess the effect of different adsorption parameters by using the CCD-RSM methodology.

The use of the fractal BSf model (n,α) gives information about the sorption strength, the half-life time and the rate as function of time, to characterize and classify the adsorbate-adsorbent couple. The equation of BSf (n,α) takes into consideration the complexity of the adsorption process [35]. It has been used in several references [36,37]. The fifth objective in this paper was to model adsorption kinetics and equilibrium using the nonlinear fit of Brouers-Sotolongo equations. To our knowledge, this is the first comprehensive study that has evaluated the synergetic optimization of pollutants removal and data modelization using Brouers-Sotolongo family models.

Batch adsorption experiments of CIP and MB were carried out to discuss the biosorption kinetics, isotherms, and thermodynamics, and possible adsorption mechanisms were also accordingly proposed.

1. Materials and methods

1.1 Chemicals

Ciprofloxacin (CIP) and Methylene blue (MB) were respectively purchased from Panreac AppliChem and Loba Chemie Pvt. Ltd. and used without additional purification. The 1-Butyl-3-methylimidazolium chloride (BMIMCl) was purchased from abcr GmbH.

Table 1S illustrates the chemical structures and some properties of CIP antibiotic, MB dye and BMIMCl as ionic liquid.

Table 1S.

Stock solutions of CIP (70 mg/L) and MB (200 mg/L) were prepared by mixing 70 mg and 200 mg of the antibiotic and the dye, respectively in 1L of distilled water. Then the working concentrations were daily prepared by suitable dilution.

1.2 Biosorbent preparation

In this work the adsorbent was a biocomposite of 50% regenerated-reed (RR) and 50% reed-charcoal (ChR). The reed (R) *(Phragmites australis)* was obtained from marshes in Gabes (Tunisia). It was chopped off into undersized particles, and then it was cleaned with distilled water until obtaining clear wash water. The reed particles were firstly diried by simple exposure to the sun rays. Then, they were dried in an oven for 24 hours at a temperature between 323.15 K and 328.15 K. R was ground using a crusher (Retsch GmbH, Germany) and then sieved to get different size particles.

To prepare the ChR, all experiments were carried out at room temperature. First, 10g of R powder was treated with 1L of orthophosphoric acid (H_3PO_4) solution (1M) during 2 hours, at room temperature. Then, the R treated with H_3PO_4 was neutralized using ultra-pure water and NaOH solution (0.01M), until pH = 6.95 ± 0.5, to remove the excess of orthophosphoric acid. Afterwards, the dough was carbonized at 523.15 K for 2 hours in a muffle furnace in an oxygen-limited environment so as to simulate the surface soil temperatures effect on lignocellulosic materials. The oven was then cooled down to room temperature and the obtained reed-charcoal was named (ChR).

The dissolution of R in the BMIMCl is affected by several parameters such as particle size and temperature. For this reason, preliminary tests were conducted to study the effect of these two parameters. It was observed that the finer granulometry (less than 53µm) needed less time to dissolve. Besides, the optimal temperature for the dissolution was 383.15 K since it presented two advantages: improved dissolution and low energy consumption.

It is well known that the dissolution mechanism is based on the interaction between the lignocellulosic material and the ionic liquid. Cl anions form hydrogen bonds with the hydroxyl protons of cellulose and hemicellulose. At the same time, aromatic BMIM cations in the bulky imidazolium cation, prefer to associate with the oxygen free doublets of the hydroxyl groups [38]. The follow-up of the dissolution was carried out with the naked eye, by means of a laser, and by optical microscopy. The solid BMIMCl was converted to a liquid at a temperature of 383.15 K. Then, a mixture of 7.5 g of powder R and 100 g of liquid BMIMCl was stirred at 600 rpm and at a temperature of 383.15 K, for 5 hours. When the R was totally dissolved in the BMIMCl, 7.5 g of ChR was added to the solution. Thereafter, the regeneration step was performed in 1L of water.

In order to regenerate the dissolved material, based on some preliminary tests, water as an effective and economical anti-solvent was chosen. Monitoring the evolution of the pH and the conductivity of the regeneration water was a good indicator of the evolution of the regeneration process. Indeed, when the pH and the conductivity values of the regeneration water reached values close to those of water, it was concluded that the material was totally free of the BMIMCl, and the regeneration protocol was effective. Subtle changes in the structure and size of the cellulose occurred not only in the solubilization state but also in the reconstitution stage.

After regeneration, the composite was frozen at a temperature of 256.15 K; the purpose of freezing is to create pores following the formation of ice. The last step in the production of regenerated-reed/reed-charcoal (RR-ChR) composite was the lyophilization to allow the dehydration of the material by sublimation under vacuum and to preserve the pores. The RR-ChR was stocked in desiccators for later use.

1.3 Characterization methods

The isoelectric point (pH_{pzc}) of RR-ChR was obtained following Razmovski, Pus and Vuc's powder addition method [39]. 0.15g of adsorbent was added to 50 mL of 0.01M NaCl

solution. The initial pH was fixed between 1 and 12 by adding either 0.1 M HCl and/or NaOH. Then the suspension was equilibrated, at a temperature of 295 K, for 24h. The final pH was recorded by an Orion Star A211 pHmeter (Thermo Fisher Scientific, USA). In line with Chan et al. [40], the point of zero charge (pH_{pzc}) was considered the point where pH_{final} is equal to $pH_{initial}$. To determine the chemical composition of materials, Fourier Transform Infrared Spectroscopy (FTIR) measurements were considered. This characterization was realized by a Spectrum Two spectrophotometer (PerkinElmer, USA), in the attenuated total reflection (ATR) mode. The corresponding detector was a deuterated triglycine sulfate (DTGS) detector. The samples were scanned in the 450–4000 cm^{-1} wave number range, with a 2 cm^{-1} spectral resolution. A scanning electron microscope (SEM) (Model: Philips Co., Netherlands) was used to examine the biosorbents morphology and elucidate the adsorption mechanism. The specific surface areas of adsorbents were calculated by the N_2-BET (Nitrogen - Brunauer–Emmett–Teller) adsorption test (Micrometrics Instrument Corp., USA). Thermo-gravimetric measurements (TGA/DTG) of samples were also performed, using a thermogravimetric analyzer (TGA/DSC3+, Mettler Toledo), under inert gas N_2, 100 ml/min, and with a heating rate of 10 K/min. The samples were heated from 303.15 to 1173.15 K. The amounts of the analyzed R, ChR and RR-ChR samples were about 26.846, 30.290 and 22.188 mg, respectively.

1.4 Analytical methods

The concentration of the CIP antibiotic and the MB dye in the solution was determined spectrophotometrically (UV-visible spectrophotometer, PG Instruments Ltd., UK), at the maximum wavelength (λ_{max}) 273 nm and 662 nm, respectively. However, the measurement of λ_{max} was carried out using solutions with concentrations ranging between 2.5 and 20 mg/L and 2.5 and 25 mg/L of the antibiotic and the dye, respectively.

1.5 Adsorption procedure

In this study, experiments were performed in batch mode. The biosorption study consisted in pouring a 10 mL solution of contaminants (5 mL of CIP and 5 mL of MB with double concentration) in an Erlenmeyer flask and stirring at 350 rpm, at room temperature. The central composite design (CCD) technique was used to determine the optimum biosorption conditions. The effect of temperature on the biosorption process was studied at four different temperatures: 293.15, 303.15, 313.15, and 323.15K at optimum conditions determined by

CCD. The concentrations of CIP and MB in the solution were determined spectrophotometrically.

The amount of contaminant adsorbed at time t, q_t (mg/g) and at equilibrium q_e (mg/g) were obtained by adopting Zhu et al.'s [41] and Akar et al.'s [42] respective equations (1) and (2) :

$$q_t=(C_0 - C_t)V/m \quad (1)$$

$$q_e =(C_0 – C_e)V/m \quad (2)$$

The dye removal percentage (% R) was determined according to equation (3) [43]:

$$\% R= 100(C_0-C_e)/C_0 \quad (3)$$

where C_0, C_t, and C_e (mg/L) are the liquid-phase concentrations of solutes; at the initial time, at any time t, and at equilibrium, respectively; V is the volume of solution (L) and m is the adsorbent dosage (g).

The kinetic study was performed in Erlenmeyer flasks containing 200 mL of the antibiotic and dye binary solution, stirred at 350 rpm, at T = 303.15 ± 1K, and at the determined optimum conditions. The concentrations of pollutants were measured at distinct times varying from 5 to 150 min.

1.6 Error analysis

In order to choose the adequate kinetic and isotherm models for the adsorption phenomenon the non-linear regression coefficients (R^2), the Person's Chi-square statistic (χ^2) and the residual sum of squares (RSS)were calculated using equations (4) and (5):

$$X^2 = \frac{Y_i - f(x_i, \hat{\theta})}{\sigma_i} \quad (4)$$

$$\mathrm{RSS}\left(\mathrm{X}, \hat{\theta}\right) = \sum_{\mathrm{i}=1}^{\mathrm{n}} [\mathrm{Y_i} - \mathrm{f}(\mathrm{x_i'}, \hat{\theta})]^2 \quad (5)$$

where, Y is the general non-linear model. $\mathrm{X} = (\mathrm{x_1}, \mathrm{x_2}, \ldots, \mathrm{x_k})'$ is the independent variable. $\theta = (\theta_1, \theta_2, \ldots, \theta_k)'$ is the parameter. $\mathrm{x_i'}$ is the row vector for the ith (i = 1, 2, ..., n) observation.

1.7 Experimental design

The results of the experimental design obtained by CCD under response surface methodology (RSM) were statically analyzed using STATISTICA 12.0 software in order to determine the optimum adsorption conditions [44]. The removal of both pollutants was realized using batch binary biosorption experiments. The response surface methodology (RSM) based on the central composite design (CCD) allows optimizing the experimental conditions and minimizing the number of experiments [45]. The effect of all studied factors and the interaction between the controlled parameters on the response (adsorption percentage) were assessed using CCD [3].

In the present work, the independent variables were the mass of adsorbent (X_1 : 0.75-1.25 g/L), the CIP concentration (X_2 : 20-50 mg/L), the MB concentration (X_3 : 50-100 mg/L), the pH (X_4 : 4-8) value and the contact time (X_5 : 35-85 min). The mentioned narrow range of adsorbent mass was used to save materials. The decision to limit the CIP concentration values between 20 and 50 mg/L and those of MB between 50 and 100 mg/ was guided by the fact that the antibiotic and the dye were found in wastewater at low concentrations. The experimental optimization was conducted in a large range of pH (acid medium and basic medium). Some preliminary studies showed that the CIP and the MB adsorption process was rapid. Therefore, the time range chosen for this study was 35 to 85 min.

The regression analysis was conducted in function of the values revealed by the experiments. A non-factorial central composite orthogonal design was performed using 5 replicates of center points, 10 star (axial) points, and 32 cube (factorial) points; so the total number of experiments was 47.

Each parameter was coded at 5 levels designed as follows: the lowest (-α), the low level (-1), the center point level (0), the high level (+1) and the highest level (+α). **Table 1** represents the interval corresponding to each level for both pollutants. The axial distance α is the distance of the star points from the center of the design.

Table 1

For a central orthogonal composite design, the axial distance α was calculated using equation (6):

$$\alpha = \left[\left(\sqrt{n_c + n_0 + n_0} - \sqrt{n_c}\right)^2 * \frac{n_c}{4}\right]^{\frac{1}{4}} \qquad (6)$$

where n_c is the number of cube points in the design, n_s is the number of star points in the design, and n_0 is the number of center points in the design.

The mathematical correlation between the selected independent variables and the response can be expressed by the second order polynomial model that was formulated by Ghafari et al.'s [46] equation (7):

$$Y = b_0 + \sum_{i=1}^{k} b_i X_i + \sum_{i=1}^{k} b_{ii} X_i X_i + \sum_{i=1}^{k} \sum_{j=i+1}^{k} b_{ij} X_i X_j \qquad (7)$$

where, Y represents the predicted response (predicted removal percentage); b_0, b_i, b_{ii} and b_{ij} are the model constant, the linear coefficient, the quadratic (squared) coefficients, and the cross-product coefficient, respectively; and X_i, X_j are the independent variables.

Table 2S illustrates the experimental design points (factorial points, axial points, and central points) and the results for binary adsorption of the antibiotic and the dye. The five central points allow determining the duplication of the experimental data.

Table 2S

1.8 Kinetic models

Nonlinear data and derivatives spectra were carried out using OriginPro. 8.5 for Windows. The family of kinetics Brouers-Sotolongo model, based on the Burr-XII statistical distribution [47], is the most widespread fractal theory studied in the domain of kinetics adsorption of contaminants onto porous materials [48]. The statistical macroscopic model BSf (n,α) broadly integrates fractal diffusion and adsorption, irreversibility, and the nature of the nascence and ending (birth-death or sorption-desorption mechanism) of the procedure [49,50]. In the present study, Brouers–Sotolongo fractal BSf equation (n,α) was used in order to depict the biosorption kinetic data of the antibiotic and dye binary adsorption onto RR-ChR as was recommended in several previous works [36,37].

The BSf (n,α) was expressed following Musawi, Brouers and Zarrabi's [49] equation (8)

$$q_{n,\alpha}(t) = q_e\left[1 - \left(1 + (n-1)\left(\frac{t}{\tau_{n,\alpha}}\right)^{\alpha}\right)^{\frac{-1}{n-1}}\right] \qquad (8)$$

where $q_{n,\alpha}(t)$ and q_e are the adsorbed dye amounts (mg/g) at time t (min) and at equilibrium, respectively, n is the fractional reaction order, α represents the fractal time index related to the adsorption and the fractal diffusion kinetics depending on the energetic and geometrical

heterogeneity of the adsorbent, and $\tau_{n,\alpha}$ is the characteristic time of the adsorption kinetics expressed by equation (9).

$$\tau_{n,\alpha} = (k_{n,\alpha}(q_e)^{n-1})^{\frac{-1}{\alpha}} \qquad (9)$$

The use of the deformed n-exponential leads to Brouers and Sotolongo-Costa's [47] equation (10).

$$Exp_n(x) = [1-(n-1)x]^{\frac{-1}{n-1}} \qquad (10)$$

The BSf (n,α) model can thus be written as follows :

$$q_{n,\alpha}(t) = q_e[1-\mathrm{Exp}_n(-(\frac{t}{\tau_{n,\alpha}})^{\alpha})] \qquad (11)$$

The required time to sorb half of the maximum adsorbed amount $\tau_{1/2}$, expressed by equation (13), was obtained from the Brouers' [51] equation (12):

$$\frac{1}{2} = [1+(n-1)(\frac{t}{\tau_{n,\alpha}})^{\alpha}]^{\frac{-1}{n-1}} \qquad (12)$$

with

$$\tau_{1/2} = \tau_{n,\alpha}(\frac{2^{(n-1)}-1}{n-1})^{\frac{1}{\alpha}} \qquad (13)$$

Five approximate equations can be taken from the general BSf equation (n,α) by giving particular values to n and α.

The five models are indicated below:

When n = 1 and α = 1, the pseudo-first-order (PFO) model is obtained,

$$q(t) = q_{e,1}[1-\mathrm{Exp}(-\frac{t}{\tau_{1,1}})] \qquad (14)$$

where $\tau_{1,1} = k_1^{-1}$, $\tau_{1/2} = \log(2)$ and $k_1$is the adsorption rate constant of the pseudo-first-order model (min^{-1}).

The pseudo-first-order model implies that the adsorption phenomenon is reversible [52]. In addition, this model supposes that the rate of adsorption is proportional to the difference in the concentration of saturation and the number of unoccupied sites by the adsorbates [53].

When n = 2 and α = 1, the pseudo-second-order (PSO) model is obtained

$$q(t) = q_{e,2}\left(\frac{\frac{t}{\tau_{2,1}}}{1+\frac{t}{\tau_{2,1}}}\right) \quad (15)$$

where $\tau_{2,1} = (q_{e,2}k_2)^{-1}$, $\tau_{1/2} = \tau_{2,1}$ and k_2 is the adsorption rate constant of the pseudo-second-order model (g.mg^{-1} min^{-1})

The pseudo-second order (PSO) equation is used to describe the kinetics of the pollutant binding reaction on the adsorbent. The PSO model assumes that the rate of adsorbates uptake is directly proportional to the square of the number of unoccupied sites. [53] The PSO model shows that the adsorption mechanism is insured by chemisorption, which includes the exchange of energy between the adsorbent and the adsorbate [54].

When, n =1 and α≠1, we get the Weibull kinetics (also named Avrami kinetics or Weibull fractal first-order models) as follows:

$$q(t) = q_{e,W}\left[1 - \mathrm{Exp}\left(-\left(\frac{t}{\tau_{1,\alpha}}\right)^{\alpha}\right)\right] \quad (16)$$

with $\tau_{1,\alpha} = k_{1,\alpha}^{-1}$ and $\tau_{1/2} = \tau_{1,\alpha}(Ln2)^{\frac{1}{\alpha}}$, and $k_{1,\alpha}$is the adsorption rate constant of the weibull model (min^{-1}).

The weibull kinetic equation defines certain kinetic parameters, such as the possible modifications of the adsorption rates as a function of the initial contaminant concentration and the biosorption time, and determines the fractional kinetic orders [54].

When n =2 and α≠1, one attains the Hill kinetics (also named Hill fractal second-order kinetics) as follows

$$q(t) = q_{e,H}\left(\frac{\left(\frac{t}{\tau_{2,\alpha}}\right)^{\alpha}}{1+\left(\frac{t}{\tau_{2,\alpha}}\right)^{\alpha}}\right) \quad (17)$$

with $\tau_{2,\alpha} = (q_{e,H}k_{2,\alpha})^{-1}$, $\tau_{1/2} = \tau_{2,\alpha}$ and $k_{2,\alpha}$ is the adsorption rate constant of the Hill model (g.mg^{-1} min^{-1}).

The Hill's model has been extensively used for the study of the relationships of the sigmoidal dose effect in several applications, such as pharmacological, physiological, and biochemical contexts [49].

It is important to note that the order n is very difficult to assign using BSf (n,α). This is due to the fact that the limited numbers of data prevent the determination of the accurate value of the asymptotic exponent ($\frac{\alpha}{n-1}$) [49].

In a data series, some are better represented by BSf (1,α) and some others by BSf (2,α) with very close regression parameters (R^2). Consequently, it has been proposed to apply BSf (1.5,α) for the entire series [55]. Furthermore, the adsorption order (n) depends on the experimental conditions that were not taken into account in the present study. In that event, the two parameters α and $\tau_{1/2}$ would be more responsible for the macroscopic description of the adsorption process and would allow a more accurate classification of adsorbent-adsorbate systems for industrial procedures [56].

Equation (18) shown below corresponds to the BSf (1.5,α) kinetics called the Brouers–Gaspard kinetics:

$$q(t) = q_{e,BG}[1 - (1 + 0.5(\frac{t}{\tau_{1.5,\alpha}})^{\alpha})^{-2}] \quad (18)$$

with

$$\tau_{1/2} = \tau_{1.5,\alpha}[2(\sqrt{2} - 1)]^{\frac{1}{\alpha}} \quad (19)$$

This equation presents all the authentic statistical functions properties with the good asymptotic properties. The use of the BSf (1.5,α) kinetic model facilitates the establishment of a comparison between data having the same precision degree.

Considering that the kinetics data provide an interesting idea for modeling and designing the biosorption procedure, kinetic adsorption results can be analysed to figure out the adsorption reaction dynamics with a focus on the constant rate order. It is important to note that the conditions used in the kinetic studies are the optimum biosorption conditions determined by the CCD design. The kinetic results were analyzed employing six different kinetic models: BSf, PFO, PSO, Hill, Avrami and BG equations. The consistency between the predicted and the experimental values was evaluated using the coefficients of correlation (R^2). In addition, the kinetic model appropriateness was verified by the reduced Chi-square (χ^2) and the residual sum of square (RSS).

1.9 Adsorption isotherms

In light of some mathematical and statistical considerations, and by attributing well-defined values to the form parameters (a) and (c), the normal Brouers–Sotolongo (BS), Freundlich, Jovanovich, Hill–Sips (HS), Langmuir and Brouers Gaspard (BG) isotherms can be acquired from the General Brouers–Sotolongo (GBS) equation [57].

The GBS equation (20) is expressed as follows:

$$q_{e,GBS} = q_{e,max}\left(1 - Exp_c\left[-\left(\frac{C_e}{b}\right)^a\right]\right) = q_{e,max}\left(1 - \left[1+c\left(\frac{C_e}{b}\right)^a\right]^{\frac{-1}{c}}\right) \quad (20)$$

where $q_{e,GBS}$ and $q_{e,max}$ are the adsorbed amount at equilibrium and the saturation adsorbed amount at equilibrium respectively (mg/g) and C_e is the adsorbate concentration in the liquid phase (mg/l). The coefficients (a) and (c) are related to the form and (b) represents a scale parameter [50]. The exponent (a) gives an idea about the shape and width of the adsorption energy distribution which is related to the substrate heterogeneity [57].

The knowledge of (a), (b) and (c) parameters can be used to calculate the usual statistical distribution quantities. It obeys a birth and death differential equation which was discussed in previous papers [57]. $C_{e_{\frac{1}{2}}}$ (50% of C_e) depends on the three constants a, b and c. For the GBS model, $C_{e_{\frac{1}{2}}}$ was calculated using equation (21):

$$C_{e_{\frac{1}{2}}} = b\,(\tfrac{2^c-1}{c})^{\frac{1}{a}} \quad (21)$$

- For c=0, the corresponding isotherm is the BS isotherm:

$$q_{e,BS} = q_{e,maxBS}\left(1 - Exp\left[-\left(\frac{C_e}{b}\right)^a\right]\right) \quad (22)$$

with

$$C_{e_{\frac{1}{2}}} = b\,(Ln2)^{\frac{1}{a}} \quad (23)$$

If $C_e \ll b$ (at low concentrations), the Freundlich isotherm is obtained by equation (24):

$$q_{e,F} = k_F C_e^a \quad (24)$$

The Freundlich adsorption isotherm model assumes that the surface energy is heterogeneous and the adsorbed molecules interact between them to form a pollutants poly-layer. The active sites are those having the strongest binding energies [58].

- For c=0 and a=1, the Jovanovich isotherm is obtained by equation (25)

$$q_{e,J} = q_{e,maxJ}\left(1 - Exp\left[-\frac{C_e}{b}\right]\right) \qquad (25)$$

$$C_{e_{\frac{1}{2}}} = b\,Ln2 \quad (26)$$

Hypothetically, this isotherm would imply that the decrease of the part of the unoccupied surface by the adsorbate particles is strictly proportional to a power of the adsorbate partial pressure [50,59].

- For c=1, the HS isotherm is recovered by equation (27):

$$q_{e,HS} = q_{e,maxHS}\left(1 - \left[1 + \left(\frac{C_e}{b}\right)^{a}\right]^{-1}\right) \qquad (27)$$

$$C_{e_{\frac{1}{2}}} = b \qquad (28)$$

- For c=1 and a=1, the Langmuir isotherm is obtained by equation (29) :

$$q_{e,L} = q_{e,maxL}\left(\frac{{}^{C_e}/_{b}}{1 + {}^{C_e}/_{b}}\right) \qquad (29)$$

$$C_{e_{\frac{1}{2}}} = b \qquad (30)$$

The Langmuir adsorption isotherm is based on the hypothesis of the formation of an adsorbed pollutant monolayer on a homogeneous surface. The active sites are specific, identical and homogeneous in terms of adsorption energy [60]. The Langmuir model assumes that each site can adsorb only one molecule, in the condition of the absence of any interaction between the adsorbed molecules [61].

- For c=0.5, the BG isotherm is obtained:

Brouers and Al-Musawi [62] demonstrated that the c constant must be in the range [0-1]. However, when the isotherm does not access saturation, the c value may be higher than 1. In this case, the result has no physical signification in a statistical approach. Since it is hard to

decide whether to select c=0 (HS isotherm) or c=1 (BS isotherm), Brouers suggested the Brouers Gaspard (BG) isotherm with c=0.5, which reads as follows [63]:

$$q_{e,BG} = q_{e,maxBG}\left(1 - Exp_{c=0.5}\left[-\left(\frac{C_e}{b}\right)^{a}\right]\right) = q_{e,maxBG}\left(1 - \left[1+\frac{1}{2}\left(\frac{C_e}{b}\right)^{a}\right]^{-2}\right) \quad (31)$$

$$C_{e_{\frac{1}{2}}} = b\,(2\sqrt{2}-2)^{\frac{1}{a}} \quad (32)$$

The Dubinin-Radushkevich (D-R) adsorption isotherm model is illustrated by equation (33):

$$q_{e,DR} = q_{e,maxDR}\left(1 - Exp\left[(-K_{DR}\ln(1+\frac{1}{C_e}))^2\right]\right) \quad (33)$$

where, $q_{e,maxDR}$ is the maximum adsorption capacity (mg/g). K_{DR} is the D-R isotherm constant, which is associated with the mean free energy E (kJ/mol) of adsorption [22]. E gives an idea about the nature of adsorption process [64]. If E is less than 8 kJ/mol, the adsorption phenomenon follows physisorption; while, if E is between 8 and 16 kJ/mol, the adsorption phenomenon seems to follow chemical ion-exchange [65].

E is determined by equation (34):

$$E = \frac{RT}{K_{DR}} \quad (34)$$

where R is the universal gas constant (8.314 J.mol/K) [66].

The Dubinin model is a changed form of the Freundlich model. It is used to describe the adsorption process for microporous and mesoporous materials [67].

The adsorption isotherm may describe the interaction between adsorbates and adsorbents. The equilibrium adsorption isotherm gives an idea about the adsorption system design [68,69]. It is based on the relationship between the liquid-phase equilibrium concentration (C_e) and the amount adsorbed at equilibrium per unit of mass (q_e) [2]. In the present work, adsorption data were analyzed using eight isotherm models, which are GBS, BS, Freundlich, Jovanovich, HS sips, Langmuir, BG and DR model.

2. Results and discussion

2.1 Characterization of the biosorbents

The pH_{pzc} corresponds to the pH value when $pH_{initial}$ is equal to pH_{final}. **Fig. 1** shows that the pH_{pzc} of RR-ChR is 4.8. When pH is less than pH_{pzc}, the adsorbent surface is positively charged and the adsorption of anions is favored. However, if pH is greater than pH_{pzc}, the biosorbent surface is negatively charged and adsorption of cations is favored [32,70].

Fig. 1

Fig. 2a exhibits the FTIR-ATR spectra of the R, ChR, and RR-ChR particles. The spectra of raw R and treated RR-ChR revealed the presence of the characteristic functional groups of lignocellulosic material. A medium absorption band in the range of 3650–3000 cm^{-1} attributed to C–H and O-H stretching in cellulose [70,71] and to the association of hydrogen bonds, was observed for the R, ChR, and RR-ChR spectra [72]. The FTIR spectrum of R shows a peak that occurred at 2920 cm^{-1}, which can be assigned to the symmetric C-H vibrations of cellulose and hemicelluloses. The observed peak at 2850 cm^{-1} can be related to the C-H stretching of lignin [73]. The intense peak, present in R and R-ChR spectra, near 1034 cm^{-1} originating from carbonyl peak can be related to the structure of cellulose. As was explained by Zhang et al [74] the vibration at 1635 cm^{-1} could be assigned to the C=O stretching band of a lateral chain of lignin. In addition, this peak observed at 1635 cm^{-1} was plausibly associated to the O-H band due to adsorbed water [75]. This observation that it disappeared in the spectrum of Ch-R after desorption of the absorbed water and the loss of the structural water of cellulose after carbonization at 523.15 K would likely support this latter interpretation. In line with [76], the C–C ring breathing band at 1156 cm^{-1} can be attributed to the presence of cellulose in the R and RR-ChR structure.

This peak was absent in the ChR spectrum since the carbonization causes chain breakage or depolymerization, and breaks in C-O and C-C bonds. However, this can be plausibly explained by the fact that the separate thermal decomposition of any lignocellulosic component definitely causes the decomposition of the whole material.

The R and RR-ChR FTIR spectra showed a typical peak at 1733 cm^{-1}. However, in the ChR structure, this peak was unnoticeable. In line with Ben Arfi et al. [31], this can be explained by the presence of the C=O elongation vibration of ketones, carboxylate and methyl ester groups in pectin and its absence in the ChR structure.

In the range of 1240 and 1450 cm^{-1}, peaks could be ascribed to R and RR-ChR surface structures containing C–O–H, C–O and C–H bonds related to carboxylic acids as was previously reported by Taylor et al [75].

Similarly, the appearance of a new intense peak at 1713 cm^{-1} in the ChR and RR-ChR spectra could be attributed to the C=O and CO_2 elongation vibrations obtained from the transformation of ketones, phenols, ether, esters and/or aromatic carboxylic groups as it was explained by Guedidi et al, and Alshaheri et al [77,78].

In total agreement with Guedidi and Slama [77] and Ben Arfi et al.[32], the three spectra common peak at 1600 cm^{-1} would imply the presence of an aromatic C=C bond, asymmetric COO^- or to the C=O conjugated with aromatic bonds [79]. The signals at 1509 cm^{-1} and 1595 cm^{-1} in the R and RR-ChR spectra respectively, can be attributed to C–C in plane aromatic vibrations. As was rightly inferred by Danial et al. [76], this would be an indicator of the presence of lignin. However, thermal decomposition of hemicelluloses occurred at temperatures between 473.15 and 523.15 K. Simultaneously, at 513.15 K cellulose started decomposing. Therefore, the decomposition of hemicelluloses and the partial decomposition of celluloses would be the cause of the elimination of the C–C in plane aromatic vibrations bonds at 1509 cm^{-1} and 1595 cm^{-1}.

Fig. 2b exhibits the RR-ChR, RR-ChR-CIP-MB FTIR-ATR spectra after binary adsorption of CIP and MB. As observed, CIP and MB adsorption showed OH and NH_2 peaks appearance at 1598 cm^{-1}.

This finding confirms the pollutants adsorption onto the RR-ChR surface. After CIP and MB adsorption, the decrease in the intensity of the C=O and CO_2 bands at 1715 and the C–C band at 1156 cm^{-1} were observed. After binary adsorption onto the RR-ChR surface, the band at 1487 cm^{-1}, associated to the C-C aromatic bond, shifted to 1509 cm^{-1}. In the same way, the band at 1370 cm^{-1} attributed to the C-C deformation moved to 1379 cm^{-1}. Finally, the band at 896 cm^{-1} associated to the C–C band shifted to 885 cm^{-1}. This shift may be due to the adsorption phenomenon. However, the peaks at 790-810 cm^{-1} were assigned to the S-O group confirming the MB adsorption. The band appearing at 1326 cm^{-1} may correspond to the N=O functional group undergoing the CIP adsorption. In conclusion, the appearance of new groups characteristic of the CIP and MB molecules, the increase of the intensity of some peaks and the shifts of other bands would confirm the biosorption of CIP and MB contaminants onto the RR-ChR particles.

Fig. 2

Surface area and porosity analysis were obtained on the basis of nitrogen (N_2) adsorption at T=77 K. The BET surface area and other porosity parameters of raw adsorbent and the adsorbent loaded by CIP and MB, are presented in **Table 2.** The BET surface area of RR-ChR was equal to 8.9 m^2/g, This finding confirms previous results reported by Kumari et al. obtained during Biosorption studies on shelled *Moringa oleifera* Lamarck seed powder [80] and Antunes et al. on Isabel grape bagasse [81]. Both studies revealed that biomass materials are characterized by low surface values. In addition, the average pore size of RR-Ch and RR-ChR-CIP-MB were 9.6 and 14.6 nm (in the range of 2–50 nm) respectively. In total agreement with Yu et al [82], this pore size is a sign of the presence of mesopores. Moreover, this reduction of values of the BET surface area and the total pore volume can be explained by the CIP and MB molecules occupation of the pores after the adsorption. Nevertheless, the CIP and MB biosorption capacity is not only related to the BET surface area, but also to the functional groups on the surface and the solution pH, as was indicated by Muhammad et al. [83].

Table 2

Thermo-gravimetric (TG) and derivative thermo-gravimetric (DTG) curves of R, ChR and RR-ChR are shown in **Fig. S1a, S1b** and **S1c**. TG-DTG curves of all samples show a first thermal incident at T 310.15-397.15 K, 310.15-478.15 K and 310.15-409.15 K for R, ChR and RR-ChR respectively, with a weight loss between 3.01 and 6.17% due to dehydration. Furthermore, **Fig. S1a** shows a noticeable 82.55 % weight loss in the TG-DTG curve of R at temperatures between 397.15 K and 678.15 K. In a study on the characterization of hemicellulose, cellulose and lignin pyrolysis, Yang [84] rightly interpreted such a huge weight loss by the depolymerization of hemicellulose, the breakdown of cellulose glycosidic bonds and the decomposition of lignin. However, as shown in **Fig. S1c**, the TG-DTG curve of RR-ChR showed two dips at 409.15-591.15 K and 591.15-696.15 K. In addition, this material presented a lesser weight loss than R. Indeed, RR-ChR lost only 63.38% of its weight. This could be explained by the total degradation of cellulose and hemicellulose and the partial degradation of lignin. This finding confirms Ben Arfi et al.'s [32] explanation, who indicated that the presence of several branches and aromatic rings in the lignin structure hampers its decomposition. Hence, lignin requires a wide interval of temperature from less than 473.15 K to almost 1123.15 K to be degraded. Similarly, as shown in **Fig. S1b**, the TG-

DTG curve of ChR showed a noticeable 80.69 % weight loss at temperatures between 477.15 K and 1123.15 K. This could be explained by the degradation of the remaining cellulose, hemicellulose and lignin in the materials structure after carbonization.

Fig. S1

The R, ChR and RR-ChR thermal decomposition followed three, two and four steps respectively. The LOI (limiting Oxygen Index) value was defined as the minimum concentration of oxygen [O_2] in a mixture of oxygen/nitrogen [O_2/N_2], which is sufficient to sustain the combustion of the polymer. It was calculated using the Van Krevelen's [85] equation.

$$LOI = 17.5 + 0.4C_Y \qquad (35)$$

where C_Y is the char yield (% wt) at T= 1123 K.

Table 3 shows the LOI values and temperature values of 5 and 10% weight loss (T5% and T10%) of R, ChR and RR-ChR samples. In function of $T_{10\%}$ and LOI values, ChR seemed to be more thermally stable and better flame-retardancy than R and RR-ChR. The lower $T_{5\%}$ value of ChR can be explained by the presence of a large amount of H_2O molecules. In addition, all the samples presented LOI values above 21%, indicating that R, ChR and RR-ChR possess some degree of self-extinguishing behavior. This finding confirms Mallakpour et al [86,87], who theorized that the burning of these materials cannot be accomplished without an external energy involvement.

Table 3

Fig. 3 illustrates the porosity of the biosorbent surface through SEM images of RR-ChR surface before and after adsorption. **Fig. 3a1, a2, a3** exhibit a clear sight of the pores at the surface of the adsorbent. Similarly, the SEM micrograph of RR-ChR revealed an irregular structure, rough and porous surface. The RR-ChR surface morphology appeared to possess an uneven structure and porous cavities. With these characteristics, the RR-ChR surface morphology can be considered very adequate as an active site for the pollutants. However, its surface morphology changed considerably by CIP and MB adsorption, as shown in **Fig. 3b1, b2, b3**. Indeed, the SEM micrographs of RR-ChR-CIP-MB powder showed that the surface became smoother and more regular (but still rough) compared to RR-ChR surface morphology, indicating coverage of RR-ChR surfaces by CIP and MB molecules. The RR-

ChR surface after CIP and MB adsorption illustrates that the adsorbent pores was thoroughly covered by antibiotic and dye molecules, which characterizes the adsorption phenomena [31].

Fig. 3

2.2 Statistical analysis

According to the CCD application, the relationships between the efficient removals, as response, and the input variables were estimated by quadratic empirical polynomial models. Below are the equations corresponding to CIP and MB binary removal:

$$\begin{aligned} Y_{(\%R\,CIP)} = 9.27 + 5.94X_1 - 2.66X_2 - 8.35X_3 + 7.31X_4 + 1.06X_5 - 1.37X_1^2 - 1.96X_2^2 \\ + 3.30X_3^2 + 8.22X_4^2 - 1.47X_5^2 - 4.01X_1X_2 - 6.15X_1X_3 + 3.93X_1X_4 \\ + 1.21X_1X_5 + 3.72X_2X_3 - 2.47X_2X_4 - 0.27X_2X_5 - 4.91X_3X_4 \\ - 1.33X_3X_5 - 1.21X_4X_5 \end{aligned} \quad (36)$$

$$\begin{aligned} Y_{(\%R\,MB)} = 65.60 + 13.44X_1 + 1.45X_2 - 16.21X_3 + 9.636X_4 + 2.78X_5 - 0.70X_1^2 \\ + 2.29X_2^2 - 2.08X_3^2 + 0.32X_4^2 - 1.47X_5^2 + 0.01X_1X_2 + 0.59X_1X_3 \\ - 2.54X_1X_4 - 0.81X_1X_5 + 2.68X_2X_3 - 0.14X_2X_4 - 0.46X_2X_5 \\ - 3.21X_3X_4 - 0.66X_3X_5 + 0.81X_4X_5 \end{aligned} \quad (37)$$

where, X_1, X_2, X_3, X_4, and X_5 are the adsorbent mass (g/L), the CIP concentration (mg/L), the MB concentration (mg/L), the pH and the contact time (min).

Negative coefficients for existing components in the model indicate the adverse effects on the removal, whereas, positive coefficients indicate favorable effects on the removal efficiency of the antibiotic and the dye.

As can be seen in **Table 3S**, the relevance of the statistical model was evaluated by the Fisher test (F-value) of each parameter at 95% confidence interval. The factor having probability values (P-values) lesser than 0.05 was considered significant within a 95% confidence level.

Table 3S

The factors significance in the model was described using the Pareto graph. According to Saad, Tahir and Ali [88], the principle of Pareto stipulated that most model influences are met by some significant factors**. Fig. S2** shows the two Pareto Charts of CIP and MB removal. **Fig. S2a** shows that the MB concentration was the most important factor for the CIP removal

from the binary solution of antibiotic and dye. In addition, the quadratic and linear pH factors, the adsorbent dosage, the interaction of adsorbent mass and MB concentration, the interaction between MB concentration and pH, were additional significant factors for the CIP removal. Similarly, **Fig. S2b** shows that the MB concentration was the most important factor for the MB removal. As shown by S. Mirzadeh et al, the chemical structure of the used dyes is one of the most important factors with a significant impact on the decolorization percentage [89]. The adsorbent amount and the pH were additional significant factors.

Fig. S2

Table 4 summarizes the results of the ANOVA analysis keeping only the significant results where p was lesser than 0.05 [90]. In line with Asfaram et al. [91,92], these would be also visible on a Pareto chart. Therefore, the empirical models of %R CIP and %R MB can be expressed by the following equations:

$$Y_{(\%R\ CIP)} = 9.27 + 5.93X_1 - 2.66X_2 - 8.35X_3 + 7.31X_4 - 1.96X_2^2 + 3.30X_3^2 + 8.22X_4^2 - 4.01X_1X_2 - 6.15X_1X_3 + 3.93X_1X_4 + 3.72X_2X_3 - 2.47X_2X_4 - 4.91X_3X_4 \quad (38)$$

$$Y_{(\%R\ MB)} = 65.60 + 13.44X_1 - 16.21X_3 + 9.636X_4 + 2.78X_5 + 2.29X_2^2 - 2.54X_1X_4 + 2.68X_2X_3 - 3.21X_3X_4 \quad (39)$$

The models correctness and goodness were statistically justified by the regression coefficients. The values of R^2 of the second-order empirical polynomial models were obtained as shown in **Table 4**.

Table 4

Fig. 4a, b show the diagnostic plots of the predicted values compared to the observed values. These plots would help to test the satisfactoriness of the model. These two graphs show a suitable agreement between the experimental data and that obtained with the models. As a result, the predictive model can be applied to navigate in the design space determined by the analysis of CCD.

Fig. 4

2.3 Effect of independent variables as counter plots and response surface

This study conducted a three-dimensional response surface plots as a function of two factors at time, while all other independent variables were kept at fixed optimal levels in order to help in understanding their main and the interaction effects [93]. **Fig. 5** shows the 3D representation of the CIP and MB adsorption at the RR-ChR surface. **Fig. 5a** and **Fig. 5b** exhibit a 3D view of the RR-ChR response surface efficiency to remove CIP and MB in function of mass and time. It seems that percentages removal increase with an increase in the mass of RR-ChR. This can be explained by the fact that the adsorbent having a higher weight offers a higher surface area, which increases its removal efficiency. However, it was observed that the removal of MB depended on the reaction time. Indeed, the increase in MB removal at higher reaction time was rightly explained by Asfaram et al [91] in the following terms. RR-ChR increased in function of time. Therefore, the longer the reaction lasts, the more surface sites for binding and accumulation of MB dyes becomes available. Whereas, it can be clearly inferred that the impact of the adsorbent mass is more important than that of the reaction time in the CIP biosorption case. To account for this behavior, it should be noted that as the RR-ChR mass increases, the removal percent increases while with increasing contact time CIP removal percent decreases only marginally.

Fig. 5c and **Fig. 5d** show the effect of CIP and MB concentrations on the efficiency of the adsorbent to remove them. It seems that the initial antibiotic and dye concentrations strongly affected RR-ChR efficiency. Indeed, it was observed that the CIP and MB removal percentages decrease with increasing initial pollutant concentrations. This can be explained by the fact that strong concentrations of contaminants saturate the surface area of the adsorbent and prevent its absorbance capacity.

Finally, **Fig. 5e** and **Fig. 5f**, show the combined effect of adsorbent weight and pH on CIP and MB biosorption efficiency. Firstly, it was observed that the increase of RR-ChR weight resulted in an increase in CIP and MB removal. This can be explained by the obvious fact that more surface of adsorbent provides more active adsorption sites. However, lower amounts of RR-ChR yielded significantly lower removal percentages, which confirms our previous interpretation. Indeed, the reduction of reactive sites would result in lower ratio of pollutants molecule to vacant sites and therefore lesser removal. Secondly, the increase in pH from 4.8 to 12 seemed to enhance the MB removal efficiency. This can be due to the attraction of cationic dye onto to negative surface of RR-ChR in this pH region. In contrast, higher pH value decreased CIP biosorption. This can be explained by the existing electrostatic repulsion between cationic CIP molecules and positive adsorbent surface at low pH.

To sum up, **Fig. 6** shows that the adsorption of MB seemed to be noticeably faster than that of CIP. Hence it can be concluded that the RR-ChR adsorbent was more efficient in the removal of MB than for CIP.

Fig. 5

2.4 Optimization by the desirability function (DF) for adsorption process

Fig. 6 shows the profiles for the predicted values and the desirability option used to determine the optimum conditions for the binary adsorption process. To define the desirability of responses, it is necessary to specify the DF for each response (%R). The scale from 0 (undesirable) to 1 (highly desirable) provides the global function that must be maximized based on an efficient choice and optimization of the independent variables. The desirability of 0.5 corresponds to mean adsorption percentage.

Fig. 6

Asfaram et al defined desirability as an objective function of any specified response that may be used in better way in applications for optimization of parameters [92]. As can be seen in **Fig. 6**, the maximum response values under the optimized conditions were found to be 76.66% and 100% for CIP and MB, respectively, and desirability of 1.0. The mean adsorption values were 38.62% and 57.78% of CIP and MB, respectively. The minimum adsorption value of CIP was 0.58% while that of MB it was 15.57%. Since desirability 1.0 was chosen to be the target value, the global response given by these curves with the present level of each model variable was also indicated in **Fig. 6**. It is clear that the independent variables simultaneously influence the response and the desirability. Based on a desirability score of 1, the maximum adsorption percentages of 76.66% and 100% for CIP and MB respectively, were achieved under the optimal conditions defined as follows: 1.55 g/L adsorbent , 35 mg/L CIP, 75 mg/L MB, pH 10.42 and 115.28 min contact time. The validity of dual content experiments at the optimum conditions was observed and a close correlation to the optimization of desirability using CCD was observed.

In addition **Fig. 6** shows the effect of RR-ChR dosage on the binary adsorption process. It can be easily observed that the removal efficiency increased with the increase of the adsorbent amount. Then it stabilized at 1.25 g/L. The adsorbent amount was statistically significant ($p<0.05$) for the adsorption of both CIP and MB. The coefficient values, namely 5.93 for CIP and 13.44 for MB represent the adsorbent rates proving that X_1, the adsorbent amount

parameter, has a positive effect on biodsorption. Indeed, as was demonstrated by Manna et al. [94], a rapid increase in removal efficiency (%R) was due to a high number of available active sites. However, a high adsorbent dosage can create agglomeration. Consequently, the diffusional path length increases and the total surface area decreases. Özer et al. [95] explained this phenomenon by the fact that dye ions cannot access easily the adsorption sites. Optimization analysis shows that the adsorbed percentage of the two contaminants was stable with desirability of 1 when the initial concentrations of CIP and MB were below 35mg/L and 75mg/L, respectively. Then, the removal efficiency decreased with the increase of initial concentration. The initial concentration of CIP was a significant and unfavorable variable for the CIP removal but it was a non-significant factor for MB removal. However, the initial MB concentration was a significant and unfavorable variable for the adsorption of the two used contaminants. At higher initial concentrations, a competition occurred between the antibiotic and the dye molecules to enter in the active sites.

The CCD analysis shows that the solution pH played an important role in the adsorption phenomenon of CIP and MB ions. It was a significant and favorable factor since its p value was <0.05 and had positive coefficient for MB removal. PH factor was also found to be favorable for CIP removal. Consequently, the increase in pH values had a positive effect on CIP and MB adsorption from binary aqueous solutions. The adsorption of CIP and MB onto RR-ChR was more favored in an alkaline solution. This observation confirms previous findings by Qin et al. [96] who demonstrated that at pH higher than the pHzpc, the adsorbent surface is negatively charged. Therefore, the adsorption phenomenon is ensured by the electrostatic attraction between the cationic MB dye and the adsorbent, explaining the increase in the adsorption efficiency. On the contrary, at low pH ($pH<pH_{zpc}$), the RR-ChR surface is positively charged, an electrostatic repulsion takes place. Ben Arfi et al. [31], further explained that in this pH range, the MB adsorption process is controlled by hydrophobic interactions and/or the π-π stacking interaction.

However, Jalil et al. [97] explained CIP removal differently. They argued that whereas the CIP species are present in their cationic form at low pH values, they are present in their anionic form at higher pH values. This causes repulsive interactions between the adsorbent surface and the antibiotic. Consequently, the highest adsorbed amount of CIP may be related to other adsorption mechanisms, such as porosity, hydrophobic interactions, π-π stacking interaction and/or formation of complex between adsorbed MB and CIP.

Finally, contact time effect was assessed as an independent variable. It was found to be a statistically insignificant ($p>0.05$) factor with a positive coefficient value. This would imply that the CIP and MB biosorption was not affected by the increase in contact time. In addition, the kinetic study revealed that the rapid phase of adsorption occurred within the first 10 min for MB while that of CIP occurred within 60 min. Then, this was followed by a state of equilibrium, at the optimum biosorption conditions. Low et al. [98] rightly explained this rapid uptake by the availability of active sites on RR-ChR at the initial time. Thus a higher amount of antibiotic and dye are adsorbed.

2.5 Nonlinear kinetic modeling of antibiotic and dye adsorption

As can be seen in **Fig. S3**, all kinetic data were determined from the non-linear fit of the six models. **Table 5** and **Table 4S** illustrate them. **Fig. S3** shows an initial state where a rapid biosorption occurred up to a state of equilibrium for the two treated contaminants with a particular focus on MB. Indeed, **Fig. S3** shows that the equilibrium states were reached at 60 min and at 10 min for CIP and MB, respectively. Moreover, at equilibrium adsorption efficiency values were 17.3 mg/g and 47.4 mg/g for CIP and MB, respectively.

Fig. S3

In the six kinetic models, all the R^2 values were greater than 0.98860 and 0.99996 for CIP and MB respectively, suggesting that the kinetic equations provided a good adequacy for the biosorption of both contaminants. By comparing the R^2 values, the CIP biosorption mechanism seemed to be accurately described by the BSf model. In addition, the obtained 17.3 mg/g experimental value of CIP adsorption and the predicted 17.5mg/g value of maximum adsorption capacity (q_m) were very close. For the MB biosorption the R^2 value of BSf, weibull, Hill and BG models were all equal to 1. Yet, the comparison of the X^2 values shows that the most accurate description of the biosorption mechanism was obtained by the Hill equation. The BSf model, being a general model that includes all the other ones, presented a good agreement with the MB adsorption process although the RSS values were below and the q_m values were closer to the experimental ones.

Table 5

Fits were applied for various values of n (1, 1.5 and 2). The R^2 parameters of all used models were very high, although on the basis of the coefficient of determination (R^2) and the Chi-square (χ^2), the best nonlinear fits for both CIP and MB biosorption were observed with the

order n =2. For both contaminants, the Hill model (n=2) led to the best fit. The Hill isotherm model is used to describe the binding of various molecules onto adsorbent surface by supposing that the ligand binding ability at one site on the adsorbent macromolecule may influence various binding sites on the same macromolecule [99]. Several authors [36,51,100] agreed with that when the α constant is higher than 1. The kinetics of CIP and MB adsorption were not clearly fractal. Moreover, Brouers and Al-Musawi [63] explained the great geometric heterogeneity of the RR-ChR surface by the fact that the fractional order (n) and the fractal exponent (α) are inversely proportional to the characteristic time τc.

Table 4S

2.6 Equilibrium isotherms for dye adsorption

Fig. S4 shows the different fits of CIP and MB binary biosorption data at the optimum conditions, defined by CCD design, on RR-ChR according to the previously mentioned models. **Tables 6** and **5S** contain all parameters associated with the models. Based on the R^2 coefficient values, the Freundlich, HS sips, Langmuir, BG and DR models were not suitable for adjusting the adsorption isotherms of CIP and MB. The GBS, BS and Jovanovich models seemed more adequate, although the Jovanovich and BS models yielded better fits for CIP and MB biosorption, respectively.

Fig. S4

Table 6

The c exponent was related to agglomeration on the adsorbent surface. In other words, the c constant can give an idea about the heterogeneity degree of the adsorbent surface. Indeed, Stanislavsky et al asserted that the c value and the heterogeneity of surface are inversely proportional [101]. As shown in **Table 5S**, the variation of the c constant of the GBS equation affected the fitting quality.

Table 5S

The adjustments were made with c = 0, 0.5 and 1. Hence, the best fit, yielding the highest R^2 determination coefficients, was obtained with the Jovanovich and BS models for the adsorption of CIP and MB respectively, where c was equal to 0. Hypothetically, the Jovanovich isotherm would imply that the decrease of the part of the unoccupied surface by the pollutants particles is strictly proportional to a power of the adsorbate partial pressure

[50,59].The BS isotherm was specifically used to describe the high heterogeneous and complex systems. This model considers a pattern of sorption energy distribution makes, that is why it is suitable to depict adsorption process implying sorbing materials even if they show various chemical and structural characteristics. Biosorbent surface is assumed to be made of a finite number of patches of sites of different sorption energies [63].

By varying a and b during fitting, the adsorption isotherms of CIP and MB onto RR-ChR were correctly reflected by the BS isotherm model (c= 0). In total agreement with previous findings by Brouers and Al-Musawi [63], this study considers it (the fact that c = 0) as signs of the great heterogeneity of the RR-ChR surface, the existence of active sites and heterogeneous biosorption interactions. Furthermore, a correlation between the constants a, b and c derived from the GBS isotherm adsorption model was clearly observed. In addition, the constant (c) and the exponent a were inversely proportional to the scale parameter (b). Hence, the higher value of the (a) exponent constant confirmed the great heterogeneity of RR-ChR surface. As was explained by Brouers and Al-Musawi [63], the heterogeneity of a material stems from its chemical composition. The chemical nature of heterogeneity is caused by several functional groups, such as carbonyls, carboxyls, lactones, phenols, aldehydes, anhydride, ether and quinone amines, and other delocalized electrons inherent to the acidic/basic RR-ChR composition. However, other researchers such as Jagiello and Olivier [102], Ncibi et al. [103] and Brouers and Marquez-Montesino [50] explained the heterogeneity of materials by their geometric structures related to various morphologies, shapes and sizes of pores as well as cracks and troughs. For CIP, the fact that the parameter (a) was higher than 1 would explain the observed slow initial biosorption kinetics. Consequently, active sites would have dissimilar energy. In contrast, for MB, the parameter (a) was less than 1, which explains the initial rapid biosorption kinetics. In addition, this may be an indicator of the existence of active sites able to adsorb many molecules. It was in agreement with previous reports, Brouers [51], Brouers and Marquez-Montesino [50] and Brouers and Al-Musawi [63], who rightly argued that the exponent (a) is a good indicator of the fractal characteristics of the heterogeneous surface and its corresponding biosorption mechanisms.

The D-R modeling shows that for CIP and MB, E values were equal to 1.290 and 7.071 kJ/mol, respectively. For both pollutants E was less than 8 kJ/mol. Hence, it can be concluded that the physisorption was the main phenomenon involved in the pollutant’s uptake.

Table 7. summarizes the results reported in previous works for the adsorption of CIP and MB on different adsorbents, and compares them to the results obtained in this work. It shows that firstly, whereas most of the reported studies were conducted a in single system, experiments in the present study were performed in a binary system. Secondly, the adsorption capacity of the RR-ChR was higher than the results obtained by using other adsorbents. This would present this material as a good adsorbent for binary CIP and MB.

Table 7.

2.7 Biosorption thermodynamics

Thermodynamics of binary CIP and MB adsorption by RR-ChR were used to assess the spontaneity, exothermic or endothermic nature of the biosorption phenomenon at the adsorbate–adsorbent interface. Thermodynamic parameters (Gibbs free energy, ΔG^0, free calculated energy, ΔG^0_{cal}, enthalpy, ΔH^0, and entropy, ΔS^0 of biosorption) were calculated using the Equations (40), (41), (42), (43), and the plotting ln K_d against 1/T as follows [91,104,105]:

$$\Delta G^0 = \Delta H^0 - T\Delta S^0 \quad (40)$$

$$\Delta G^0_{cal} = -RT \ln K_d \quad (41)$$

$$K_d = \frac{q_e}{C_e} \quad (42)$$

$$\ln K_d = \frac{\Delta S^0}{R} - \frac{\Delta H^0}{RT} \quad (43)$$

where T is the absolute temperature (K), K_d is the distribution coefficient [106], R is the universal gas constant (8.314 J/mol.K) [107]. The linear plot of lnK_d versus 1/T is shown in **Fig. S5.**

Fig. S5

All thermodynamic parameter values are exhibited in **Table 8**. The negative ΔG° values at various temperatures demonstrate that the reaction is thermodynamically feasible and indicate the spontaneous nature of the adsorption [108]. The increase in negative ΔG° values and K_d

values with an increase in temperature shows an increase in feasibility of biosorption at higher temperatures. This would imply that temperature promotes the adsorption of antibiotic and dye particles through the improvement of the surface uptake capacity.

The ΔH^0 values are 46.01 kJ/mol and 37.59 kJ/mol, for CIP and MB biosorption, respectively. For both pollutants, the fact that ΔH^0 is positive indicates that adsorption has an endothermic nature in the temperature range considered. Moreover, the ΔH^0 values were lesser than 80 kJ/mol. Therefore, the adsorption of CIP and MB onto RR-ChR is typical of physical biosorption. This result corroborates with the D-R model analysis findings.

The ΔS^0 values are 163.38 J/mol.k and 165.47 J/mol.k, for CIP and MB biosorption, respectively. The positive values of ΔS^0 suggest the increased randomness at the solid/solution interface during the adsorption of CIP and MB by RR-ChR. Similar results were obtained in other thermodynamic studies concerning adsorption of dyes onto different biomaterials [91,105].

Finally, the comparison of the ΔG^0 and ΔH^0 values, corresponding to CIP and MB, revealed the faster adsorption of MB, due to the stronger interactions and more affinity between the RR-ChR adsorbent surface and MB molecules. This finding confirms the isotherms analysis.

Table 8.

2.8 Proposed Adsorption mechanisms

RR-ChR is a composite between regenerated reed and charcoal of reed, and the Reed is of natural origin. RR is composed of celluloses, hemicelluloses and lignins. The ChR was obtained by carbonization of treated reed by ortho-phosphoric acid. The chemical heterogeneity of the adsorbent surface was confirmed by the FTIR analysis, as well as kinetic and isotherm studies. Both components of RR-ChR biocomposite were rich in hydroxyls, carbonyls, ethers, phenols, aldehydes, and aromatic compounds.

The results showed that the optimum pH was equal to 8. As was explained by Bazrafshan et al, at this high pH, the carboxylic groups of RR-ChR are ionized and the negative charge density on the surface increases resulting in negative charge of the RR-ChR surface [109]. Consequently, biosorption of the MB ions occurs, through electrostatic attraction between the MB cationic groups ($R\text{-}N^+$) and the adsorbent surface. At this pH, due to resonance, the dispersed positive charge in MB ($R\text{-}N^+$) is expected to have a weak electrostatic interaction

with the (C-O$^-$) and (COO$^-$) sites in the adsorbent. The CIP pKa_1 and pKa_2, were 5.9 and 8.89, respectively. At pH 8, CIP would be negatively charged and electrostatic repulsion between the CIP anionic groups (COO$^-$) and the RR-ChR surface, would take place. The adsorption of CIP and MB would take place via hydrophobic interactions, as well as π-π stacking, as depicted in **Fig. 7**. The possible interactions between CIP and MB molecules and the adsorbent include Van der Waals interactions, and π-π stacking interaction between the benzene rings of two pollutants and the delocalized -electron system of the adsorbent. As shown in **Fig. 7**, the probable uptake mechanism of CIP followed predominantly hydrogen bonds between the proton in CIP molecules and an electronegative atom in the adsorbent surface.

According to the CCD application, the MB concentration was found to be a significant and unfavorable variable for the adsorption of the two used contaminants. This result may be caused by a stable complex formation reaction between CIP and MB. The formation of a complex would be caused by an electrostatic interaction between the cationic MB and the anionic group (COO$^-$) of CIP and/or π-π stacking interactions. In addition, the explanation of CIP and MB adsorption by the mechanism of porosity would be equally possible.

Fig. 7

Conclusion

In conclusion, this study attempted to fulfill a four-fold objective. Firstly, an enhanced biosorbent from a Tunisian reed (*Phragmites australis*), an invasive plant that abounds in Southern Tunisian marshes, was developed. The produced adsorbent would be easier to produce, more efficient and cost effective, compared to existing adsorbents. Secondly, a detailed characterization of the charcoal reed, regenerated reed and "regenerated-reed/charcoal-reed" powders produced from Phragmites australis, was conducted. It was found that these were made of cellulose, hemicellulose and lignin, which indicate their potential as good adsorbents.

But above all, the main experimental contribution of this study would be the optimization of the adsorption through the combination of five parameters; namely, the amount of contaminant, the CIP concentration, the MB concentration, the solution pH and the contact time between adsorbent and wastewater. The optimal conditions were 1.55 g/L of adsorbent, 35 mg/L of CIP, 75 mg/L of MB, a pH of 10.42 and 115.28 min contact time. This work revealed that at the mentioned optimum conditions, the removal efficiency would improve to

reach 76.66% and 100% for the removal of CIP and that of MB, respectively. Moreover, at equilibrium adsorption efficiency values were 17.3 mg/g and 47.4 mg/g for CIP and MB, respectively. Thus, the study shows that the synthesized biosorbent is effective, and economic for the simultaneous removal of CIP and MB from wastewater.

Thirdly, this study investigated and attempted to explain the adsorption mechanisms involved in this approach. The isotherm studies showed that the adsorbent surface was heterogeneous and the Jovanovich and BS models led to the most accurate nonlinear fit for the adsorption of CIP and MB, respectively. It was proved that the adsorption mechanism is physisorption; it is also spontaneous and endothermic. Possible mechanism for the CIP and MB adsorption onto RR-ChR was suggested. The biosorption mechanism was implied through porosity, through the electrostatic interaction between the cationic MB and the anionic group (COO-, OH) of adsorbent and through the Van der Waals interactions and/or π-π stacking interactions between lignin aromatic groups of RR-ChR and contaminants. These CIP and MB biosorption mechanisms were confirmed by the application of the BSf model and the Hill equation, respectively. Moreover, the efficiency of the adsorbent was studied thermodynamically and kinetically. It was found that increasing the temperature yielded a better adsorption up to 94.83 % and 99.83 % for CIP and MB, respectively, at 323.15 K. Finally, the kinetic investigation showed that although the biosorption of MB was faster than that of CIP. Indeed, results show that the equilibrium states were reached at 60 min and at 10 min for CIP and MB, respectively. There was a fast biosorption for both contaminants up to a state of equilibrium.

Our ultimate and fourth objective was to contribute to the efforts of valorizing the reed plants Phragmites australis and to improve the environmental conditions. Indeed, the proposed solution would reduce these invasive and useless plants as well as rid the environment of huge amounts of contaminated wastewaters at little expenses.

Acknowledgements The authors would like to thank the Ministry of Higher Education and Scientific Research and the University of Sfax (Tunisia) for the financial support. Authors are also grateful to Dr Ayadi Hajji for his help with editing, correcting and proofreading the English of the manuscript.

References

[1] H. Ben Mansour, O. Boughzala, dorra Dridi, D. Barillier, L. Chekir-Ghedira, R. Mosrati, Les colorants textiles sources de contamination de l'eau : CRIBLAGE de la toxicité et des méthodes de traitement, Revue Des Sciences de l'eau. 24 (2011) 209. doi:10.7202/1006453ar.

[2] R. Dutta, T. V. Nagarjuna, S.A. Mandavgane, J.D. Ekhe, Ultrafast removal of cationic dye using agrowaste-derived mesoporous adsorbent, Industrial and Engineering Chemistry Research. 53 (2014) 18558–18567. doi:10.1021/ie5030003.

[3] J.R. V Pils, D.A. Laird, Sorption of tetracycline and chlortetracycline on K- and Ca-saturated soil clays, humic substances, and clay-humic complexes, Environmental Science and Technology. 41 (2007) 1928–1933. doi:10.1021/es062316y.

[4] X. Hou, J. Liu, W. Guo, S. Li, Y. Guo, Y. Shi, C. Zhang, A novel 3D-structured flower-like bismuth tungstate/mag-graphene nanoplates composite with excellent visible-light photocatalytic activity for ciprofloxacin degradation, Catalysis Communications. (2019) 27–31. doi:10.1016/j.catcom.2018.12.006.

[5] D. Jia, D. Zhou, Y. Wang, H. Zhu, J. Chen, Geoderma Adsorption and cosorption of Cu (II) and tetracycline on two soils with different characteristics, 146 (2008) 224–230. doi:10.1016/j.geoderma.2008.05.023.

[6] S. Yang, Y. Wang, S. Lin, J. Fan, C. Liu, X. Yan, Facile surface-engineered polymeric absorbents for simultaneous adsorption and degradation of organic wastes, Chemosphere. 191 (2018) 17–22. doi:10.1016/j.chemosphere.2017.10.019.

[7] P.K. Boruah, P. Borthakur, G. Darabdhara, C.K. Kamaja, I. Karbhal, M. V. Shelke, P. Phukan, D. Saikia, M.R. Das, Sunlight assisted degradation of dye molecules and reduction of toxic Cr(<scp>vi</scp>) in aqueous medium using magnetically recoverable Fe_3O_4 /reduced graphene oxide nanocomposite, RSC Adv. 6 (2016) 11049–11063. doi:10.1039/C5RA25035H.

[8] T.O. Leiknes, The effect of coupling coagulation and flocculation with membrane filtration in water treatment: A review, Journal of Environmental Sciences. 21 (2009) 8–12. doi:10.1016/S1001-0742(09)60003-6.

[9] G.A.P. Mateus, D.M. Formentini-Schmitt, L. Nishi, M.R. Fagundes-Klen, R.G. Gomes, R. Bergamasco, Coagulation/Flocculation with Moringa oleifera and Membrane

Filtration for Dairy Wastewater Treatment, Water, Air, and Soil Pollution. 228 (2017). doi:10.1007/s11270-017-3509-z.

[10] Y. Ding, P. Zhou, H. Tang, Visible-light photocatalytic degradation of bisphenol A on NaBiO3 nanosheets in a wide pH range: A synergistic effect between photocatalytic oxidation and chemical oxidation, Chemical Engineering Journal. 291 (2016) 149–160. doi:10.1016/j.cej.2016.01.105.

[11] S. Tareq, Y. Hin, T. Yap, T.A. Saleh, A.H.A.H. Abdullah, U. Rashid, S.M. Izham, Synthesis of bimetallic gold-pallidum loaded on carbon as efficient catalysts for the oxidation of benzyl alcohol into benzaldehyde, Journal of Molecular Liquids. (2018) #pagerange#. doi:10.1016/j.molliq.2018.09.037.

[12] A. Mirzaei, L. Yerushalmi, Z. Chen, F. Haghighat, SC, Journal of Hazardous Materials. (2018). doi:10.1016/j.jhazmat.2018.07.077.

[13] G. Fadillah, A. Saleh, S. Wahyuningsih, Enhanced electrochemical degradation of 4-Nitrophenol molecules using novel Ti / TiO 2 -NiO electrodes, 289 (2019). doi:10.1016/j.molliq.2019.111108.

[14] M. Hoseini, G.H. Safari, H. Kamani, Toxicological & Environmental Chemistry Sonocatalytic degradation of tetracycline antibiotic in aqueous solution by sonocatalysis, (2014) 37–41. doi:10.1080/02772248.2014.901328.

[15] S. Raghu, C. Ahmed Basha, Chemical or electrochemical techniques, followed by ion exchange, for recycle of textile dye wastewater, Journal of Hazardous Materials. 149 (2007) 324–330. doi:10.1016/j.jhazmat.2007.03.087.

[16] A.T. Abara, C.Y. Amane, M.S. Eguchi, Adsorption Mechanism for Xanthene Dyes to Cellulose Granules Acid red, 76 (2012) 870–874. doi:10.1271/bbb.110634.

[17] T. Sismanoglu, Y. Kismir, S. Karakus, Single and binary adsorption of reactive dyes from aqueous solutions onto clinoptilolite, Journal of Hazardous Materials. 184 (2010) 164–169. doi:10.1016/j.jhazmat.2010.08.019.

[18] S.W. Lv, J.M. Liu, H. Ma, Z.H. Wang, C.Y. Li, N. Zhao, S. Wang, Simultaneous adsorption of methyl orange and methylene blue from aqueous solution using amino functionalized Zr-based MOFs, Microporous and Mesoporous Materials. (2019) 179–187. doi:10.1016/j.micromeso.2019.03.017.

[19] S. Zaidi, V. Sivasankar, T. Chaabane, V. Alonzo, K. Omine, R. Maachi, A. Darchen, M. Prabhakaran, Separate and simultaneous removal of doxycycline and oxytetracycline antibiotics by electro-generated adsorbents (EGAs), Biochemical Pharmacology. (2018) 102876. doi:10.1016/j.jece.2018.102876.

[20] H. Ding, Y. Wu, B. Zou, Q. Lou, W. Zhang, J. Zhong, L. Lu, G. Dai, Simultaneous removal and degradation characteristics of sulfonamide, tetracycline, and quinolone antibiotics by laccase-mediated oxidation coupled with soil adsorption, Journal of Hazardous Materials. 307 (2016) 350–358. doi:10.1016/j.jhazmat.2015.12.062.

[21] M. Mende, D. Schwarz, C. Steinbach, R. Boldt, S. Schwarz, Simultaneous adsorption of heavy metal ions and anions from aqueous solutions on chitosan—Investigated by spectrophotometry and SEM-EDX analysis, Colloids and Surfaces A: Physicochemical and Engineering Aspects. 510 (2016) 275–282. doi:10.1016/j.colsurfa.2016.08.033.

[22] F. Pourebrahim, M. Ghaedi, K. Dashtian, F. Heidari, S. Kheirandish, Simultaneous removing of Pb2+ions and alizarin red S dye after their complexation by ultrasonic waves coupled adsorption process: Spectrophotometry detection and optimization study, Ultrasonics Sonochemistry. 35 (2017) 51–60. doi:10.1016/j.ultsonch.2016.09.002.

[23] H. Mazaheri, M. Ghaedi, S. Hajati, K. Dashtian, M.K. Purkait, Simultaneous removal of methylene blue and Pb2+ ions using ruthenium nanoparticle-loaded activated carbon: response surface methodology, RSC Advances. 5 (2015) 83427–83435. doi:10.1039/c5ra06731f.

[24] Z. Diao, X. Xu, D. Jiang, J. Liu, L. Kong, G. Li, L. Zuo, Q. Wu, Simultaneous photocatalytic Cr (VI) reduction and ciprofloxacin oxidation over TiO 2 / Fe 0 composite under aerobic conditions : Performance , durability , pathway and mechanism, Chemical Engineering Journal. (2017) 0–41. doi:10.1016/j.cej.2017.01.006.

[25] T. Hou, H. Du, Z. Yang, Z. Tian, S. Shen, Y. Shi, W. Yang, L. Zhang, Flocculation of different types of combined contaminants of antibiotics and heavy metals by thermo-responsive flocculants with various architectures, Separation and Purification Technology. 223 (2019) 123–132. doi:10.1016/j.seppur.2019.04.068.

[26] M. Gaouar-Yadi, K. Tizaoui, N. Gaouar-Benyelles, B. Benguella, Efficient and eco-friendly adsorption using low-cost natural sorbents in waste water treatment, Indian Journal of Chemical Technology. 23 (2016) 204–209.

[27] Y. Jin, C. Zeng, Q. Lü, Y. Yu, PT, International Journal of Biological Macromolecules. (2018) #pagerange#. doi:10.1016/j.ijbiomac.2018.10.213.

[28] T.A. Saleh, Isotherm , kinetic , and thermodynamic studies on Hg (II) adsorption from aqueous solution by silica- multiwall carbon nanotubes, (2015) 16721–16731. doi:10.1007/s11356-015-4866-z.

[29] Tawfik A. Saleh, Mercury sorption by silica / carbon nanotubes and silica / activated carbon : a comparison study Taw fi k A . Saleh, Journal of Water Supply: Research and Technology—AQUA. (2015) 892–903. doi:10.2166/aqua.2015.050.

[30] P. Taylor, T.A. Saleh, Desalination and Water Treatment Nanocomposite of carbon nanotubes / silica nanoparticles and their use for adsorption of Pb (II): from surface properties to sorption mechanism, (2015) 37–41. doi:10.1080/19443994.2015.1036784.

[31] R. Ben Arfi, S. Karoui, K. Mougin, A. Ghorbal, Adsorptive removal of cationic and anionic dyes from aqueous solution by utilizing almond shell as bioadsorbent, Euro-Mediterranean Journal for Environmental Integration. 2 (2017) 20. doi:10.1007/s41207-017-0032-y.

[32] R. Ben Arfi, S. Karoui, K. Mougin, A. Ghorbal, Cetyltrimethylammonium bromide‐treated Phragmites australis powder as novel polymeric adsorbent for hazardous Eriochrome Black T removal from aqueous solutions, Polymer Bulletin. (2018). doi:10.1007/s00289-018-2648-8.

[33] Z. Parsaee, N. Karachi, S.M. Abrishamifar, M.R.R. Kahkha, R. Razavi, Silver-choline chloride modified graphene oxide: Novel nano-bioelectrochemical sensor for celecoxib detection and CCD-RSM model, Ultrasonics Sonochemistry. 45 (2018) 106–115. doi:10.1016/j.ultsonch.2018.03.009.

[34] H. Li, S. Van Den Driesche, F. Bunge, B. Yang, M.J. Vellekoop, Author ' s Accepted Manuscript, Talanta. (2018). doi:10.1016/j.talanta.2018.10.048.

[35] T. Selmi, M. Seffen, H. Sammouda, S. Mathieu, J. Jagiello, A. Celzard, V. Fierro, Physical meaning of the parameters used in fractal kinetic and generalised adsorption models of Brouers–Sotolongo, Adsorption. 24 (2018) 11–27. doi:10.1007/s10450-017-9927-9.

[36] A.M. Ben Hamissa, F. Brouers, M.C. Ncibi, M. Seffen, Kinetic Modeling Study on Methylene Blue Sorption onto Agave americana fibers: Fractal Kinetics and Regeneration Studies, Separation Science and Technology (Philadelphia). 48 (2013) 2834–2842. doi:10.1080/01496395.2013.809104.

[37] S. Gaspard, S. Altenor, N. Passe-Coutrin, A. Ouensanga, F. Brouers, Parameters from a new kinetic equation to evaluate activated carbons efficiency for water treatment, Water Research. 40 (2006) 3467–3477. doi:10.1016/j.watres.2006.07.018.

[38] B. Meenatchi, V. Renuga, A. Manikandan, Cellulose dissolution and regeneration using various imidazolium based protic ionic liquids, Journal of Molecular Liquids. 238 (2017) 582–588. doi:10.1016/j.molliq.2016.05.008.

[39] R.N. Razmovski, V.S. Pus, V.M. Vuc, Journal of the Taiwan Institute of Chemical Engineers Removal of cationic and anionic azo dyes from aqueous solutions by adsorption on maize stem tissue ˇ urovic, (2014). doi:10.1016/j.jtice.2013.12.020.

[40] S. Chan, Y. Ping, A. Halim, S. Ong, Equilibrium , kinetic and thermodynamic studies of a new potential biosorbent for the removal of Basic Blue 3 and Congo Red dyes : Pineapple (Ananas comosus) plant stem, 000 (2016) 1–10. doi:10.1016/j.jtice.2016.01.010.

[41] T. Zhu, W. Huang, L. Zhang, J. Gao, W. Zhang, Adsorption of Cr (VI) on cerium immobilized cross-linked chitosan composite in single system and coexisted with Orange II in binary system, International Journal of Biological Macromolecules. (2017). doi:10.1016/j.ijbiomac.2017.05.051.

[42] Z. Kaynak, E. Kavas, G. Incirkus, S. Tunali, T. Akar, Assessment of the biosorption characteristics of a macro-fungus for the decolorization of Acid Red 44 (AR44) dye, 171 (2009) 865–871. doi:10.1016/j.jhazmat.2009.06.085.

[43] A. Saleh, A. Sar, M. Tuzen, Chitosan-modi fi ed vermiculite for As (III) adsorption from aqueous solution : Equilibrium , thermodynamic and kinetic studies, 219 (2016) 937–945. doi:10.1016/j.molliq.2016.03.060.

[44] C. Zno, O. Fe, Magnetic dispersive micro-solid phase extraction, (2019). doi:10.1039/c8an02484g.

[45] Z. Moradi, E.A. Dil, A. Asfaram, Dispersive micro-solid phase extraction based on Fe3O4@SiO2@Ti-MOF as a magnetic nanocomposite sorbent for the trace analysis of caffeic acid in the medical extracts of plants and water samples prior to HPLC-UV analysis, (2019) 4351–4361. doi:10.1039/c9an00120d.

[46] S. Ghafari, H. Abdul, M. Hasnain, A. Akbar, Application of response surface methodology (RSM) to optimize coagulation – flocculation treatment of leachate using poly-aluminum chloride (PAC) and alum, 163 (2009) 650–656. doi:10.1016/j.jhazmat.2008.07.090.

[47] F. Brouers, O. Sotolongo-Costa, Generalized fractal kinetics in complex systems (application to biophysics and biotechnology), Physica A: Statistical Mechanics and Its Applications. 368 (2006) 165–175. doi:10.1016/j.physa.2005.12.062.

[48] F. Brouers, T.J. Al-Musawi, Brouers-Sotolongo fractal kinetics versus fractional derivative kinetics: A new strategy to analyze the pollutants sorption kinetics in porous materials, Journal of Hazardous Materials. 350 (2018) 162–168. doi:10.1016/j.jhazmat.2018.02.015.

[49] T.J. Al-Musawi, F. Brouers, M. Zarrabi, Kinetic modeling of antibiotic adsorption onto different nanomaterials using the Brouers–Sotolongo fractal equation, Environmental Science and Pollution Research. 24 (2017) 4048–4057. doi:10.1007/s11356-016-8182-z.

[50] F. Brouers, F. Marquez-Montesino, Dubinin isotherms versus the Brouers–Sotolongo family isotherms: A case study, Adsorption Science and Technology. 34 (2016) 552–564. doi:10.1177/0263617416670909.

[51] F. Brouers, The Fractal (BSf) Kinetics Equation and Its Approximations, Journal of Modern Physics. 05 (2014) 1594–1601. doi:10.4236/jmp.2014.516160.

[52] M. Ahmaruzzaman, R.A. Reza, Decontamination of Cationic and Anionic Dyes in Single and Binary Mode From Aqueous Phase by Mesoporous Pulp Waste, 00 (2014). doi:10.1002/ep.

[53] R.M. Ali, H.A. Hamad, M.M. Hussein, G.F. Malash, Potential of using green adsorbent of heavy metal removal from aqueous solutions: Adsorption kinetics, isotherm, thermodynamic, mechanism and economic analysis, Ecological Engineering. 91 (2016) 317–332. doi:10.1016/j.ecoleng.2016.03.015.

[54] A.M.M. Vargas, A.L. Cazetta, M.H. Kunita, T.L. Silva, V.C. Almeida, Adsorption of methylene blue on activated carbon produced from flamboyant pods (Delonix regia): Study of adsorption isotherms and kinetic models, Chemical Engineering Journal. 168 (2011) 722–730. doi:10.1016/j.cej.2011.01.067.

[55] S. Azizian, M. Bagheri, Enhanced adsorption of Cu 2 + from aqueous solution by Ag doped nano-structured ZnO, Journal of Molecular Liquids. 196 (2014) 198–203. doi:10.1016/j.molliq.2014.03.043.

[56] S. Douven, C.A. Paez, C.J. Gommes, Journal of Colloid and Interface Science The range of validity of sorption kinetic models, JOURNAL OF COLLOID AND INTERFACE SCIENCE. 448 (2015) 437–450. doi:10.1016/j.jcis.2015.02.053.

[57] F. Brouers, Statistical Foundation of Empirical Isotherms, Open Journal of Statistics. 04 (2014) 687–701. doi:10.4236/ojs.2014.49064.

[58] M.K. Purkait, D.S. Gusain, S. DasGupta, S. De, Adsorption behavior of chrysoidine dye on activated charcoal and its regeneration characteristics by using different surfactants, Separation Science and Technology. 39 (2004) 2419–2440. doi:10.1081/SS-120039347.

[59] L. Habana, O. Ridge, O. Ridge, Derivation and Application of a Jovanovic–Freundlich Isotherm Model for Single-Component Adsorption on Heterogeneous Surfaces ˜, 67

(1996) 57–67.

[60] A. Dalvand, R. Nabizadeh, Author ' s Accepted Manuscript, Journal of Magnetism and Magnetic Materials. (2015). doi:10.1016/j.jmmm.2015.12.040.

[61] R. Sivaraj, C. Namasivayam, K. Kadirvelu, Orange Peel as an Adsorbent in the Removal of Acid Violet 17 (Acid Dye) From Aqueous Solutions (acid dye) from aqueous solutions, 17 (2001) 105–110. doi:10.1016/S0956-053X(00)00076-3.

[62] F. Brouers, T.J. Al-musawi, Brouers-Sotolongo fractal kinetics versus fractional derivative kinetics : A new strategy to analyze the pollutants sorption kinetics in porous materials G RA P H I C A L AB S T R A C T, Journal of Hazardous Materials. 350 (2018) 162–168. doi:10.1016/j.jhazmat.2018.02.015.

[63] F. Brouers, T.J. Al-Musawi, On the optimal use of isotherm models for the characterization of biosorption of lead onto algae, Journal of Molecular Liquids. 212 (2015) 46–51. doi:10.1016/j.molliq.2015.08.054.

[64] F. Ansari, M. Ghaedi, M. Taghdiri, A. Asfaram, Application of ZnO nanorods loaded on activated carbon for ultrasonic assisted dyes removal: Experimental design and derivative spectrophotometry method, Ultrasonics Sonochemistry. 33 (2016) 197–209. doi:10.1016/j.ultsonch.2016.05.004.

[65] U.A. Guler, M. Sarioglu, Removal of tetracycline from wastewater using pumice stone: Equilibrium, kinetic and thermodynamic studies, Journal of Environmental Health Science and Engineering. 12 (2014) 1–11. doi:10.1186/2052-336X-12-79.

[66] V.A. Online, Y. Wu, J. Cao, P. Yilihan, Y. Jin, Y. Wen, J. Zhou, RSC Advances, (2013) 10745–10753. doi:10.1039/c3ra40289d.

[67] S.G. Chen, R.T. Yang, I ") & (- =, (1994) 4244–4249.

[68] E. Akbar, G. Samira, R. Abdolhossein, Evaluation of the activated carbon prepared from the algae Gracilaria for the biosorption of Cu(II) from aqueous solutions, African Journal of Biotechnology. 7 (2008) 2034–2037. doi:10.5897/AJB08.038.

[69] H. Lata, V.K. Garg, R.K. Gupta, Removal of a basic dye from aqueous solution by adsorption using Parthenium hysterophorus: An agricultural waste, Dyes and Pigments. 74 (2007) 653–658. doi:10.1016/j.dyepig.2006.04.007.

[70] N. Maaloul, P. Oulego, M. Rendueles, A. Ghorbal, M. Díaz, Novel biosorbents from almond shells: Characterization and adsorption properties modeling for Cu(II) ions from aqueous solutions, Journal of Environmental Chemical Engineering. 5 (2017) 2944–2954. doi:10.1016/j.jece.2017.05.037.

[71] J. Ma, Y. Lei, M.A. Khan, F. Wang, Y. Chu, W. Lei, M. Xia, S. Zhu, Adsorption

properties, kinetics & thermodynamics of tetracycline on carboxymethyl-chitosan reformed montmorillonite, International Journal of Biological Macromolecules. (2018) #pagerange#. doi:10.1016/j.ijbiomac.2018.11.235.

[72] J. Wang, L. Wei, Y. Ma, K. Li, M. Li, Y. Yu, L. Wang, H. Qiu, Collagen/cellulose hydrogel beads reconstituted from ionic liquid solution for Cu(II) adsorption, Carbohydrate Polymers. 98 (2013) 736–743. doi:10.1016/j.carbpol.2013.06.001.

[73] E. Science, N.M. National, Dialysis-free extraction and characterization of cellulose crystals from almond (Prunus dulcis) shells, (2016).

[74] K. Zhang, P. Sun, H. Liu, S. Shang, J. Song, D. Wang, Extraction and comparison of carboxylated cellulose nanocrystals from bleached sugarcane bagasse pulp using two different oxidation methods, Carbohydrate Polymers. 138 (2016) 237–243. doi:10.1016/j.carbpol.2015.11.038.

[75] P. Taylor, D.R. Manenti, D.E.G. Trigueros, A.P. De Oliveira, C.E. Borba, A.D. Kroumov, pt us, (2015) 37–41. doi:10.1080/09593330.2015.1051591.

[76] W.H. Danial, Z.A. Majid, M. Nazlan, M. Muhid, S. Triwahyono, M.B. Bakar, Z. Ramli, Ac ce p te d t, Carbohydrate Polymers. (2014). doi:10.1016/j.carbpol.2014.10.072.

[77] H. Guedidi, B. Slama, Préparation et modification de carbones activés pour l ' adsorption de polluants organiques émergents : molécules pharmaceutiques et liquides ioniques Hanen Guedidi To cite this version : HAL Id : tel-01407242 Préparation et modification de carbones activ, (2016).

[78] T.A.S. Ali Ahmed Alshaheri, Mohamed Ibrahim Mohamed Tahir, Mohd Basyaruddin Abdul Rahman, Thahira Begum, Synthesis, characterisation and catalytic activity of dithiocarbazate Schiff base complexes in oxidation of cyclohexane, Journal of Molecular Liquids. 240 (2017) 486--496. doi:10.1016/j.molliq.2017.05.081.

[79] A. Saleh, Simultaneous adsorptive desulfurization of diesel fuel over bimetallic nanoparticles loaded on activated carbon, (2017). doi:10.1016/j.jclepro.2017.11.208.

[80] P. Kumari, P. Sharma, S. Srivastava, M.M. Srivastava, Biosorption studies on shelled Moringa oleifera Lamarck seed powder : Removal and recovery of arsenic from aqueous system, 78 (2006) 131–139. doi:10.1016/j.minpro.2005.10.001.

[81] M. Antunes, V.I. Esteves, R. Guégan, J.S. Crespo, N. Andreia, M. Giovanela, M. Antunes, V.I. Esteves, R. Guégan, J.S. Crespo, A.N. Fernandes, Removal of diclofenac sodium from aqueous solution by Isabel grape bagasse To cite this version : HAL Id : insu-00684443, (2012).

[82] S. Yu, Y. Liu, Y. Ai, X. Wang, R. Zhang, Z. Chen, Table of Contents, Environmental Pollution. (2018). doi:10.1016/j.envpol.2018.06.031.

[83] M. Abbas, A. Zaini, M. Zakaria, S.H. Mohd, Journal of Environmental Chemical Engineering Sludge-adsorbents from palm oil mill effluent for methylene blue removal, Biochemical Pharmacology. 1 (2013) 1091–1098. doi:10.1016/j.jece.2013.08.026.

[84] H. Yang, Characteristics of hemicellulose , cellulose and lignin pyrolysis, 86 (2007) 1781–1788. doi:10.1016/j.fuel.2006.12.013.

[85] D.W. Van Krevelen, Some basic aspects of flame resistance of polymeric materials, 16 (1975) 615–620.

[86] S. Mallakpour, A. Abdolmaleki, Morphology and thermal properties of environmental friendly nanocomposites using biodegradable poly (amide – imide) based on N - trimellitylimido- S -valine matrix reinforced by fructose-functionalized multi-walled carbon nanotubes, (2014). doi:10.1007/s00396-014-3442-2.

[87] S. Mallakpour, V. Behranvand, Application of recycled PET/carboxylated multi-walled carbon nanotube composites for Cd2+ adsorption from aqueous solution: a study of morphology, thermal stability, and electrical conductivity, Colloid and Polymer Science. 295 (2017) 453–462. doi:10.1007/s00396-017-4022-z.

[88] M. Saad, H. Tahir, D. Ali, Green synthesis of Ag-Cr-AC nanocomposites by Azadirachta indica and its application for the simultaneous removal of binary mixture of dyes by ultrasonicated assisted adsorption process using Response Surface Methodology, Ultrasonics Sonochemistry. 38 (2017) 197–213. doi:10.1016/j.ultsonch.2017.03.022.

[89] S. Mirzadeh, S. Khezri, S. Rezaei, H. Forootanfar, A.H. Mahvi, M.A. Faramarzi, ENVIRONMENTAL HEALTH Decolorization of two synthetic dyes using the purified laccase of Paraconiothyrium variabile immobilized on porous silica beads, (2014) 1–9.

[90] E. Alipanahpour, M. Ghaedi, A. Asfaram, Talanta Application of hydrophobic deep eutectic solvent as the carrier for ferrofluid : A novel strategy for pre-concentration and determination of mefenamic acid in human urine samples by high performance liquid chromatography under experimental design optimization, Talanta. 202 (2019) 526–530. doi:10.1016/j.talanta.2019.05.027.

[91] A. Asfaram, M. Ghaedi, G.R. Ghezelbash, F. Pepe, Application of experimental design and derivative spectrophotometry methods in optimization and analysis of biosorption of binary mixtures of basic dyes from aqueous solutions, Ecotoxicology and

Environmental Safety. 139 (2017) 219–227. doi:10.1016/j.ecoenv.2017.01.043.

[92] A. Asfaram, H. Sadeghi, A. Goudarzi, E.P. Kokhdan, Z. Salehpour, Ultrasound-assisted combined with manganese-oxide nanoparticles loaded DOI: 10.1039/C8AN02338G on activated carbon for extraction and pre-concentration of thymol and carvacrol in methanolic extracts of Thymus daenensis, Salvia officinalis, Stachys pilifer, (2019). doi:10.1039/C8AN02338G.

[93] E.A. Dil, M. Ghaedi, A. Asfaram, F. Mehrabi, F. Sadeghfar, Graphical abstract SC, Journal of Industrial and Engineering Chemistry. (2018). doi:10.1016/j.jiec.2018.12.050.

[94] A.S. Manna, D. Roy, P. Saha, Rapid methylene blue adsorption using modified lignocellulosic materials, Process Safety and Environmental Protection. (2017). doi:10.1016/j.psep.2017.03.008.

[95] A. Özer, G. Akkaya, M. Turabik, The biosorption of Acid Red 337 and Acid Blue 324 on Enteromorpha prolifera: The application of nonlinear regression analysis to dye biosorption, Chemical Engineering Journal. 112 (2005) 181–190. doi:10.1016/j.cej.2005.07.007.

[96] Y. Qin, L. Wang, C. Zhao, D. Chen, Y. Ma, W. Yang, Ammonium-Functionalized Hollow Polymer Particles As a pH-Responsive Adsorbent for Selective Removal of Acid Dye, ACS Applied Materials and Interfaces. 8 (2016) 16690–16698. doi:10.1021/acsami.6b04199.

[97] M.E.R. Jalil, M. Baschini, K. Sapag, Removal of ciprofloxacin from aqueous solutions using pillared clays, Materials. 10 (2017) 17–19. doi:10.3390/ma10121345.

[98] L.W. Low, T.T. Teng, M. Rafatullah, N. Morad, B. Azahari, Adsorption Studies of Methylene Blue and Malachite Green From Aqueous Solutions by Pretreated Lignocellulosic Materials, Separation Science and Technology (Philadelphia). 48 (2013) 1688–1698. doi:10.1080/01496395.2012.756912.

[99] X. Yuan, Z. Wu, H. Zhong, H. Wang, X. Chen, L. Leng, L. Jiang, Z. Xiao, G. Zeng, Fast removal of tetracycline from wastewater by reduced graphene oxide prepared via microwave-assisted ethylenediamine–N,N'–disuccinic acid induction method, Environmental Science and Pollution Research. (2016). doi:10.1007/s11356-016-6892-x.

[100] F. Brouers, O. Sotolongo, F. Marquez, J.P. Pirard, Microporous and heterogeneous surface adsorption isotherms arising from Levy distributions, 349 (2005) 271–282. doi:10.1016/j.physa.2004.10.032.

[101] I. Introduction, molecular populations undergoing chemical reactions ?, (2013) 15595–15601. doi:10.1039/c3cp52272e.

[102] J. Jagiello, J.P. Olivier, 2D-NLDFT adsorption models for carbon slit-shaped pores with surface energetical heterogeneity and geometrical corrugation, Carbon. 55 (2012) 70–80. doi:10.1016/j.carbon.2012.12.011.

[103] M.C. Ncibi, S. Altenor, M. Seffen, F. Brouers, S. Gaspard, Modelling single compound adsorption onto porous and non-porous sorbents using a deformed Weibull exponential isotherm, Chemical Engineering Journal. 145 (2008) 196–202. doi:10.1016/j.cej.2008.04.001.

[104] T.A. Saleh, A.A. Al-absi, Kinetics, isotherms and thermodynamic evaluation of amine functionalized magnetic carbon for methyl red removal from aqueous solutions Tawfik, Journal of Molecular Liquids. 248 (2017) 577--585. doi:10.1016/j.molliq.2017.10.064.

[105] E. Alipanahpour, M. Ghaedi, A. Ghaedi, Application of artificial neural network and response surface methodology for the removal of crystal violet by zinc oxide nanorods loaded on activate carbon : kinetics and equilibrium study, Journal of the Taiwan Institute of Chemical Engineers. 000 (2015) 1–11. doi:10.1016/j.jtice.2015.07.023.

[106] N. Barka, K. Ouzaouit, M. Abdennouri, M. El Makhfouk, Dried prickly pear cactus (Opuntia ficus indica) cladodes as a low-cost and eco-friendly biosorbent for dyes removal from aqueous solutions, Journal of the Taiwan Institute of Chemical Engineers. 44 (2013) 52–60. doi:10.1016/j.jtice.2012.09.007.

[107] S. Yu, L. Yin, H. Pang, Y. Wu, X. Wang, P. Zhang, B. Hu, Z. Chen, X. Wang, E.X. Wang, B. Hu, X. Wang, Constructing sphere-like cobalt-molybdenum-nickel ternary hydroxide and calcined ternary oxide nanocomposites for e ffi cient removal of U (VI) from aqueous solutions, Chemical Engineering Journal. 352 (2018) 360–370. doi:10.1016/j.cej.2018.07.033.

[108] K.V. Kumar, K. Porkodi, F. Rocha, Comparison of various error functions in predicting the optimum isotherm by linear and non-linear regression analysis for the sorption of basic red 9 by activated carbon, Journal of Hazardous Materials. 150 (2008) 158–165. doi:10.1016/j.jhazmat.2007.09.020.

[109] E. Bazrafshan, F.K. Mostafapour, A.R. Hosseini, A.R. Khorshid, A.H. Mahvi, Decolorisation of Reactive Red 120 Dye by Using Single-Walled Carbon Nanotubes in Aqueous Solutions, 2013 (2013).

Figure captions

Fig. 1. Curve of pH_{PZC} of RR-ChR. Note: the blue line shown is used as a visual guide (T = 30 ± 1 °C).

Fig. 2a. FTIR-ATR spectra of the R (black line), ChR (red line), and RR-ChR (blue line)

Fig. 2b. FTIR-ATR spectra of the RR-ChR (black line) and the RR-ChR-CIP-MB (red line).

Fig. 3. SEM images of the biosorbent surface: **3a** SEM images of the biosorbent before adsorption (**a1**:*5000, **a2**: *50000, **a3**: *5000) **3b** SEM images of the biosorbent after adsorption (**b1**:*5000, **b2**: *50000, **b3**: *5000)

Fig. 4. Observed versus predicted values of dependent variables (%R) for **(a)** CIP and **(b)** MB removal (five factors : X_1, X_2, X_3, X_4, X_5 ; five blocks ; 47 runs ; T = 30 ± 1 °C).

Fig. 5. 3D surface plots for a combined effect of different independent variables for CIP and MB efficient removal. **(a, b)** Efficiency of adsorbent in function of pollutant mass and contact time (X_2 = 35 mg/L ; X_3 = 75 mg/L ; X_4 = 10.42 ; T = 30 ± 1 °C), **(c, d)** Adsorbent efficiency in function of pollutant concentrations, (X_1 = 1.55 g/L ; X_4 = 10.42 ; X_5 = 115.28 min ; T = 30 ± 1 °C), **(e, f)** Adsorbent efficiency in function of water pH and adsorbent amount (X_2 = 35 mg/L ; X_3 = 75 mg/L ; X_5 = 115.28 min ; T = 30 ± 1 °C).

Fig. 6. Profiles for predicted values and desirability function for efficient removal of CIP and MB from binary aqueous solution. Dashed red line shows the optimized values (five factors : X_1, X_2, X_3, X_4, X_5 ; five blocks ; 47 runs ; T = 30 ± 1 °C).

Fig. 7. Adsorption mechanism, Red lines: electrostatic attractions, Blue lines: hydrogen bonds, Green lines: π-π stacking interactions

Fig 1

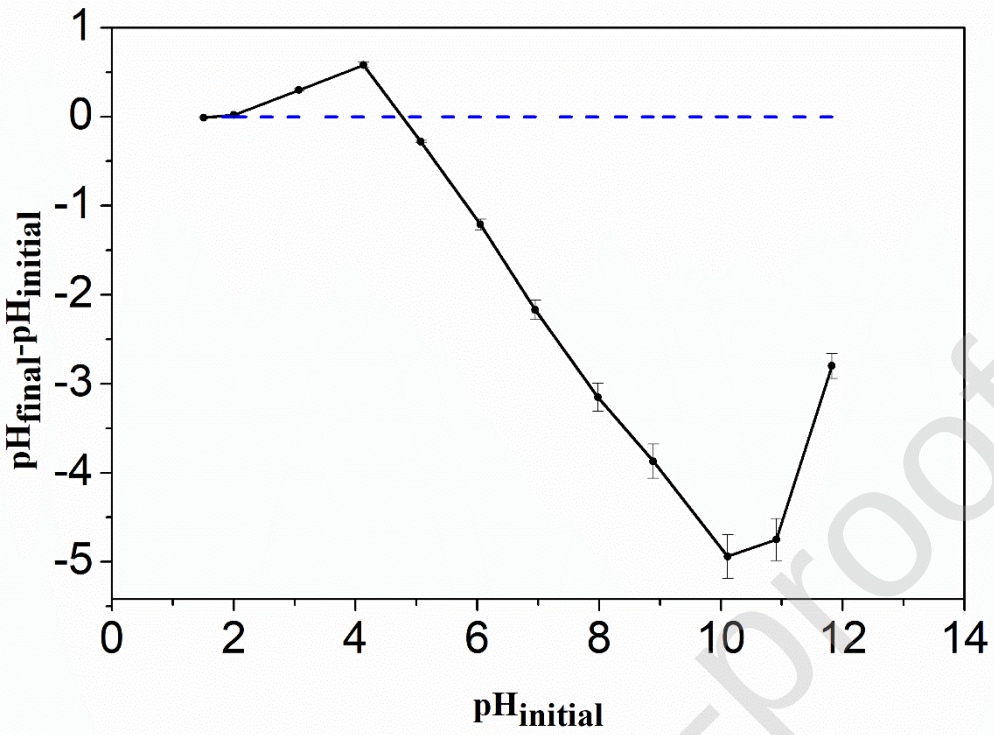

Fig 2a

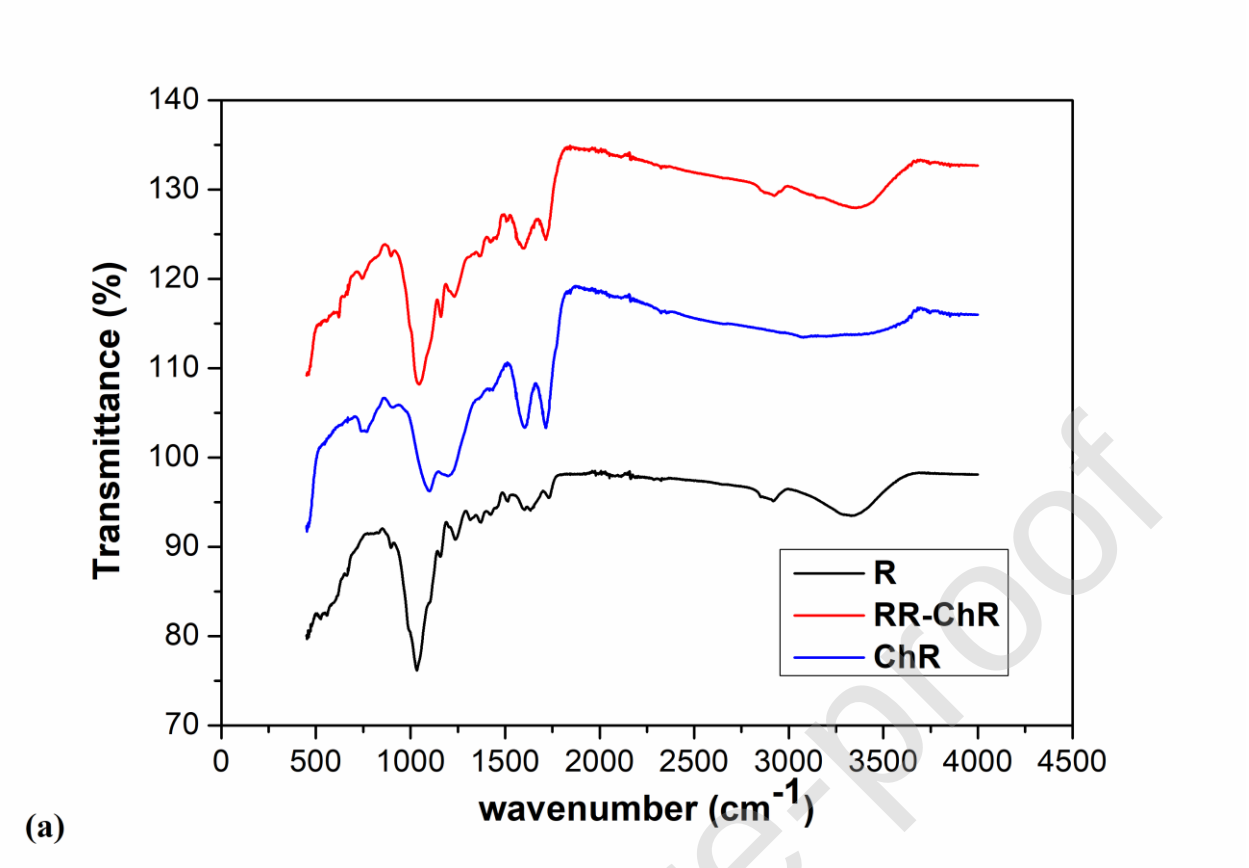

(a)

B

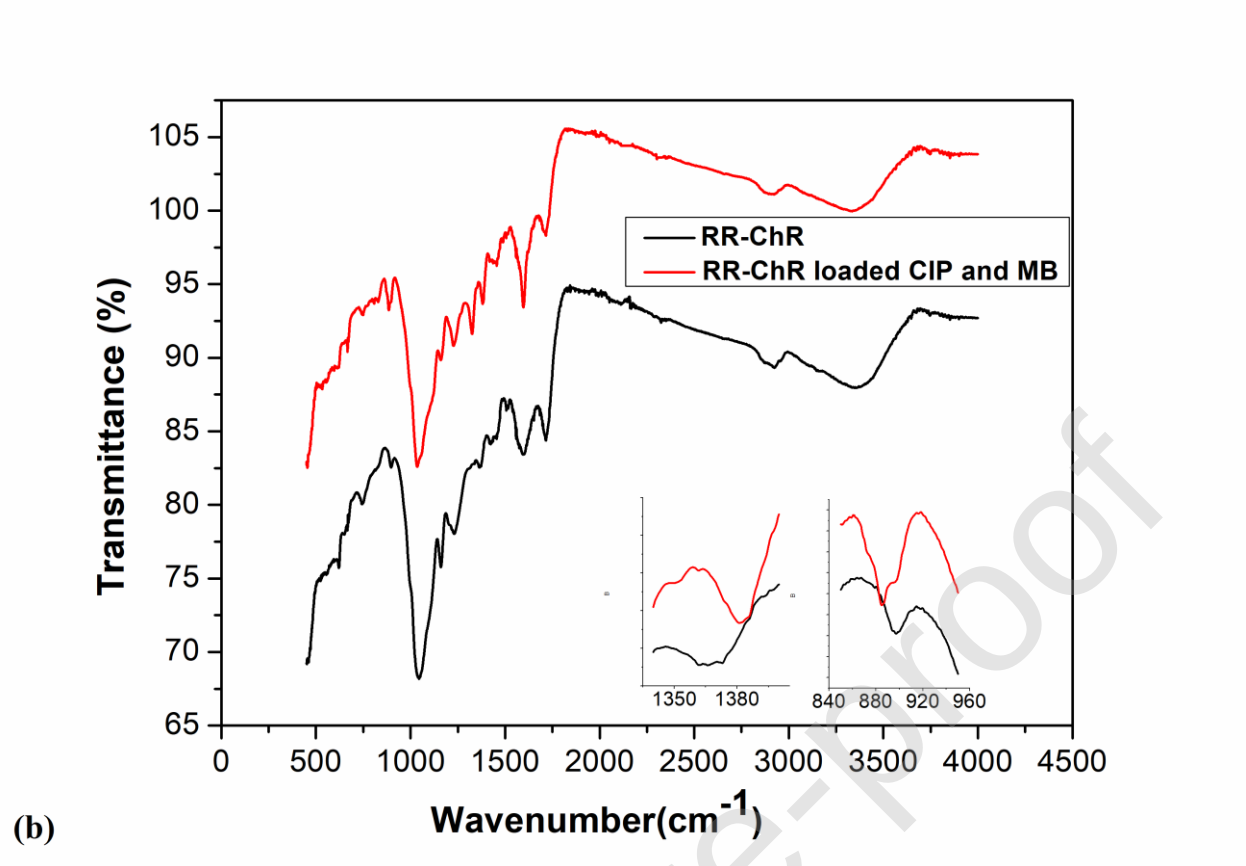

(b)

Fig 3 a1

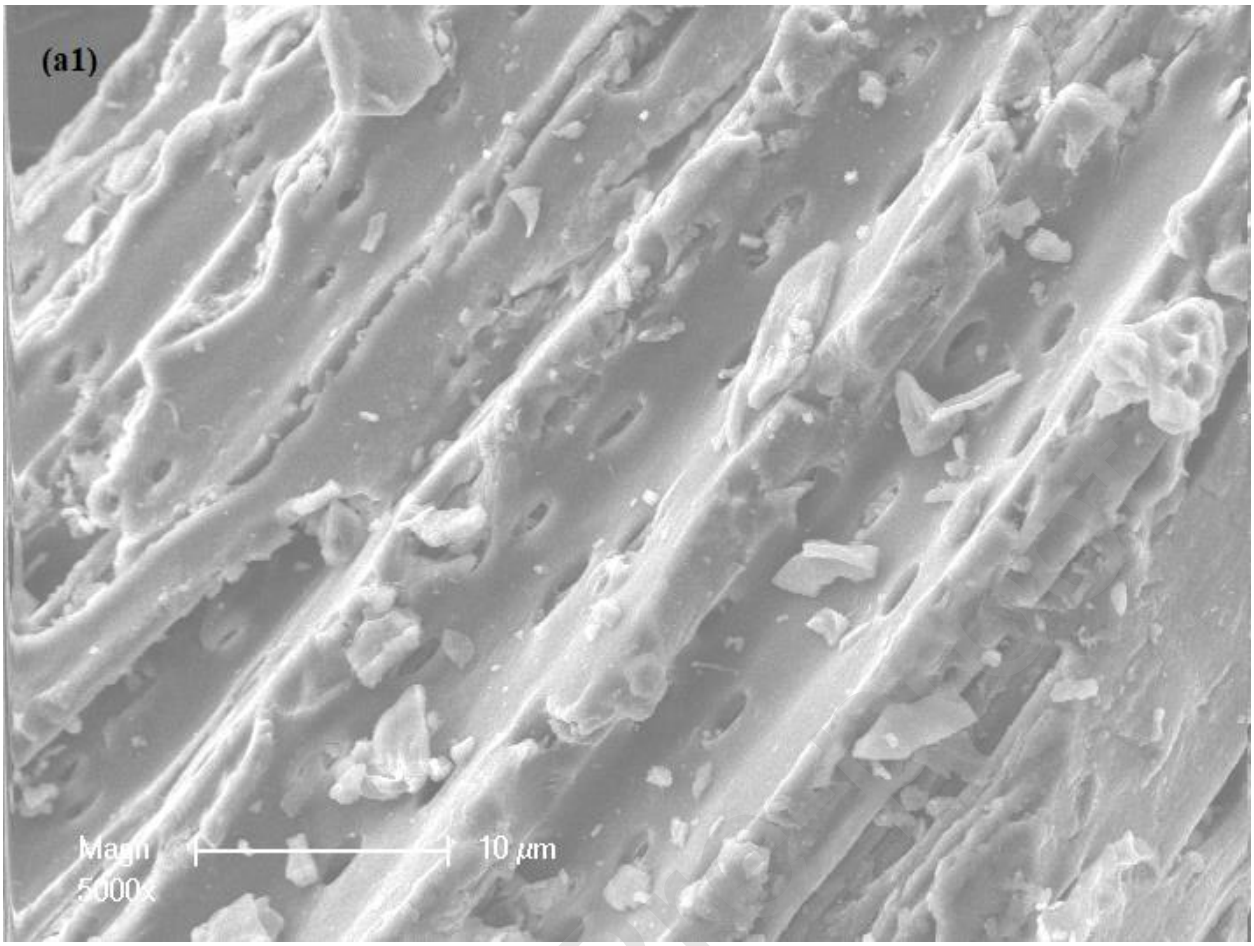

Fig 3 a2

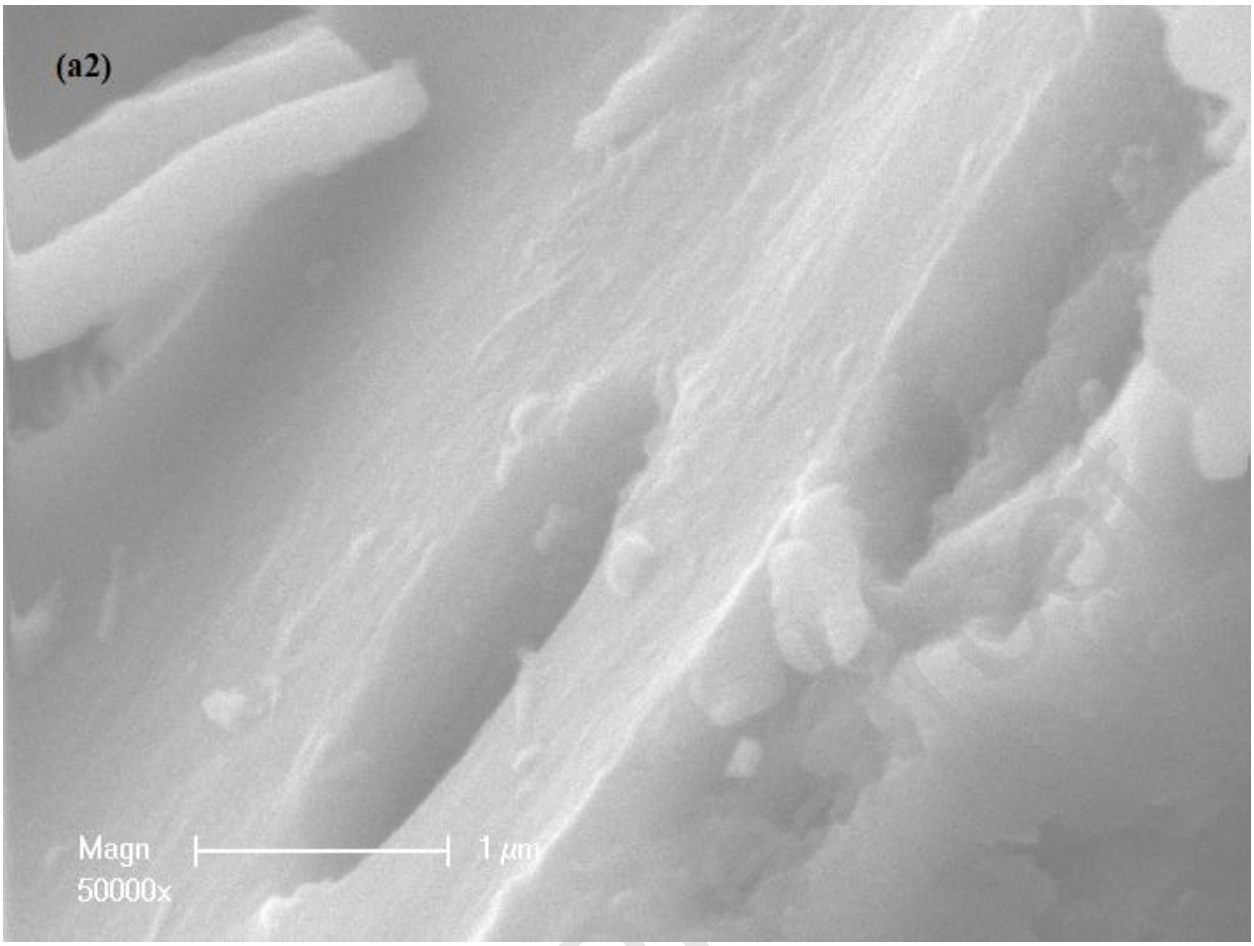

a 3

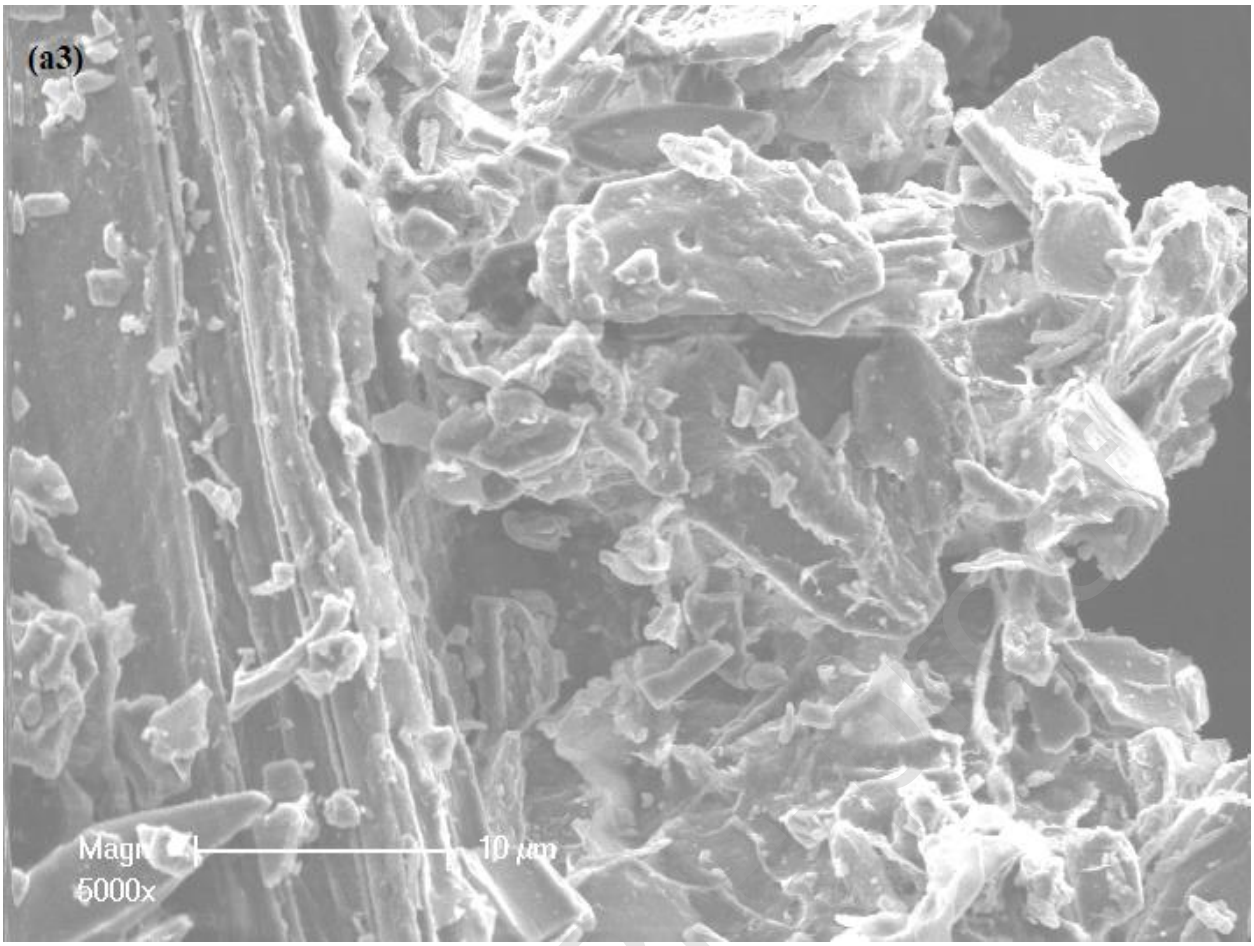

Fig 3b1

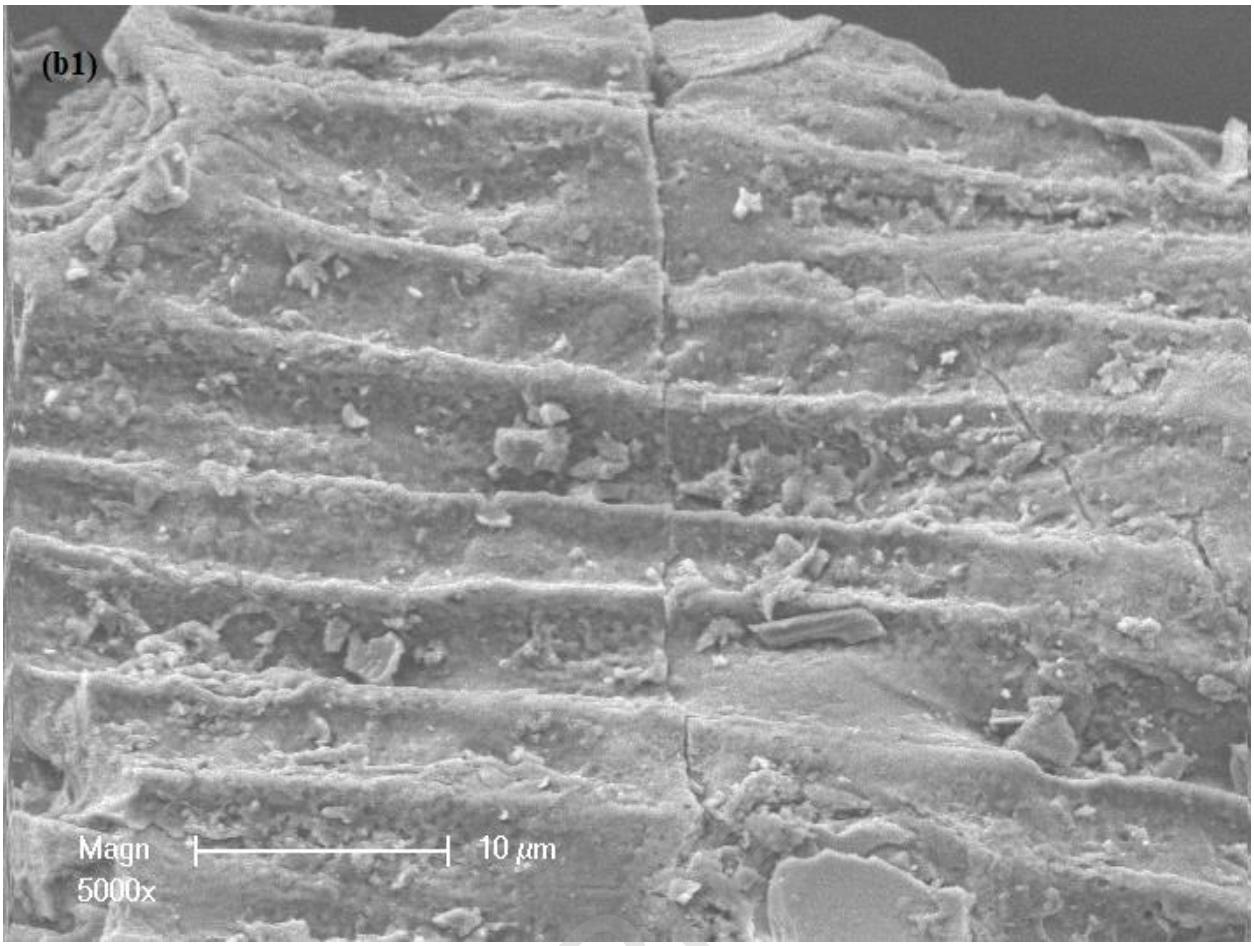

Fig 3 b2

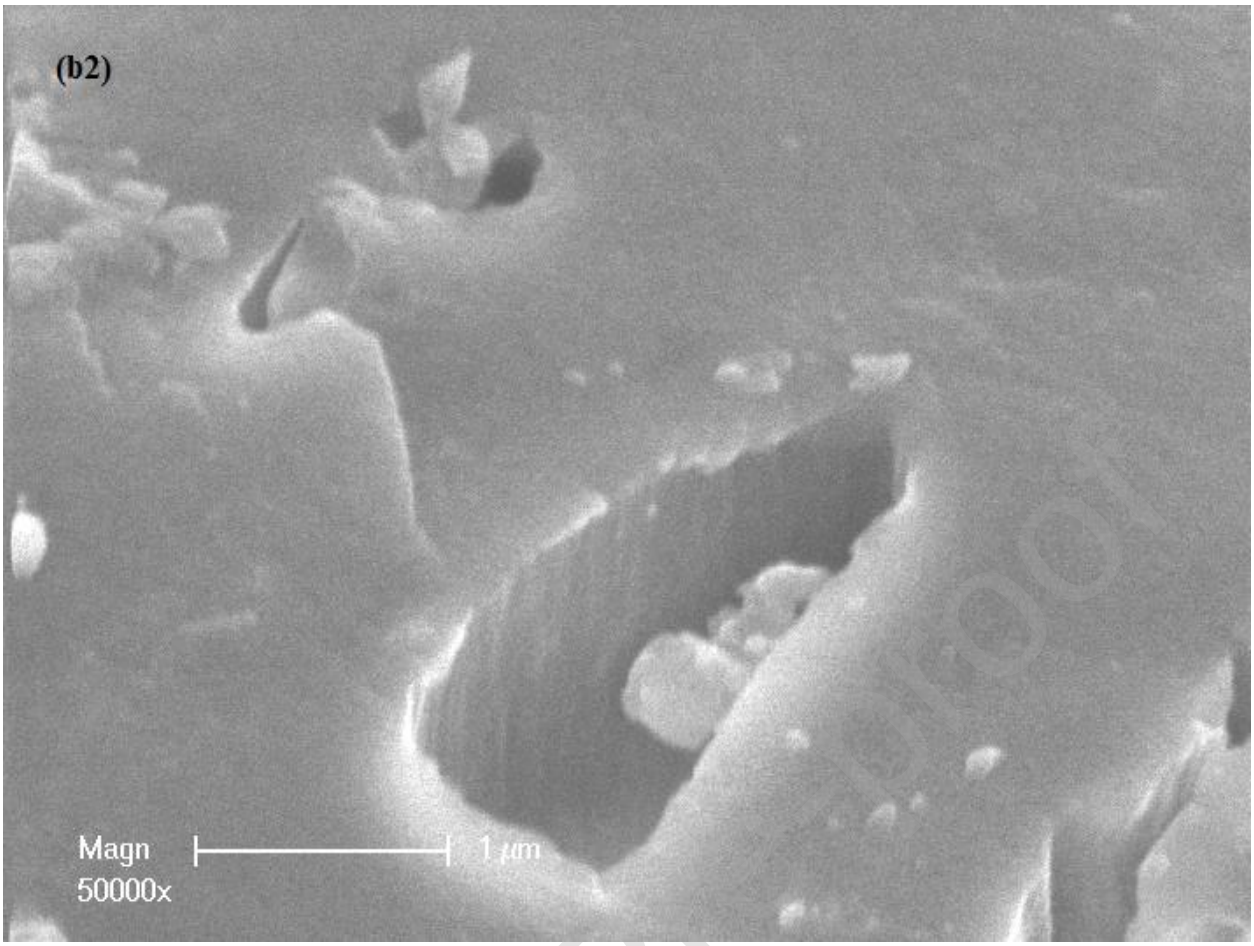

Fig b3

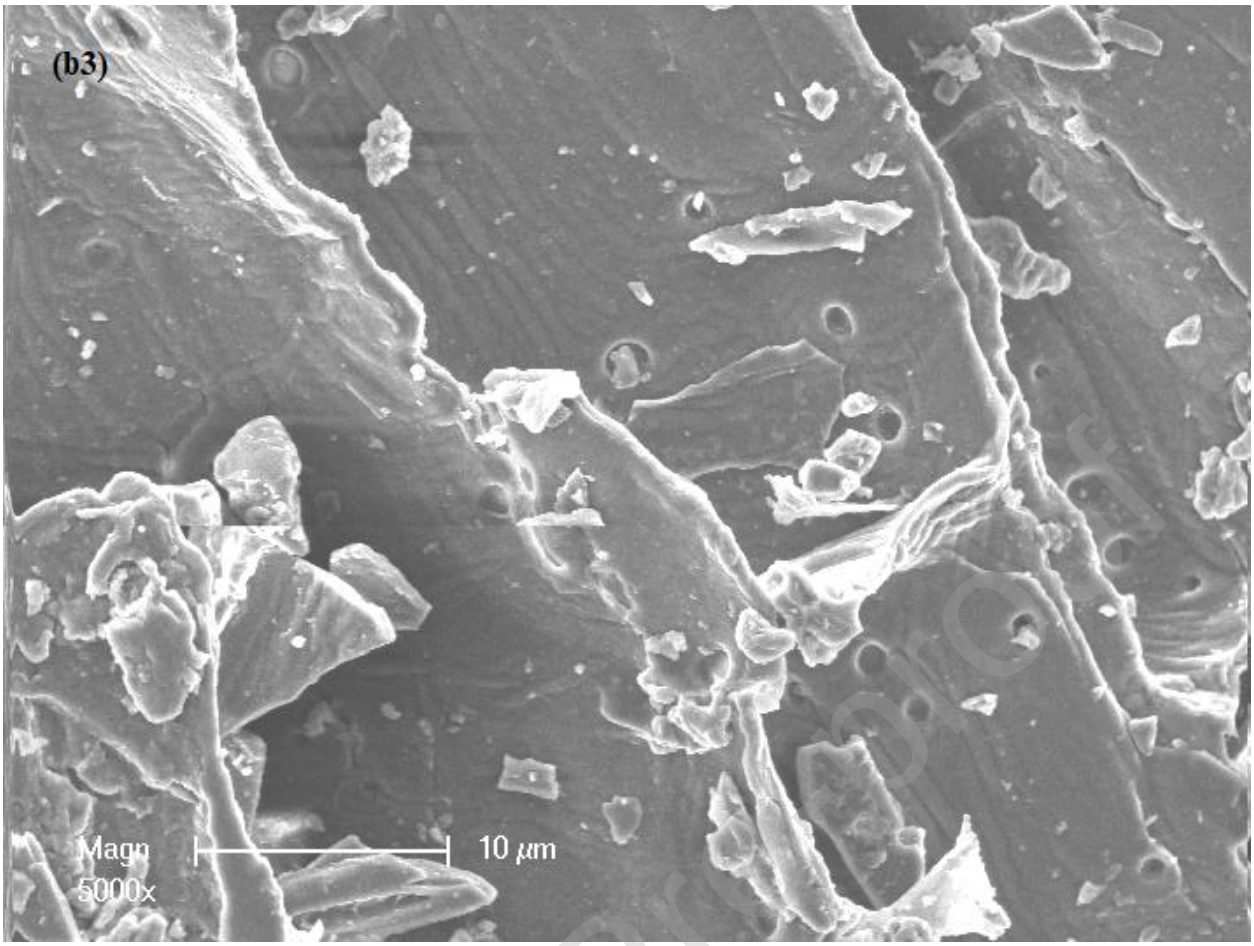

Fig 4a

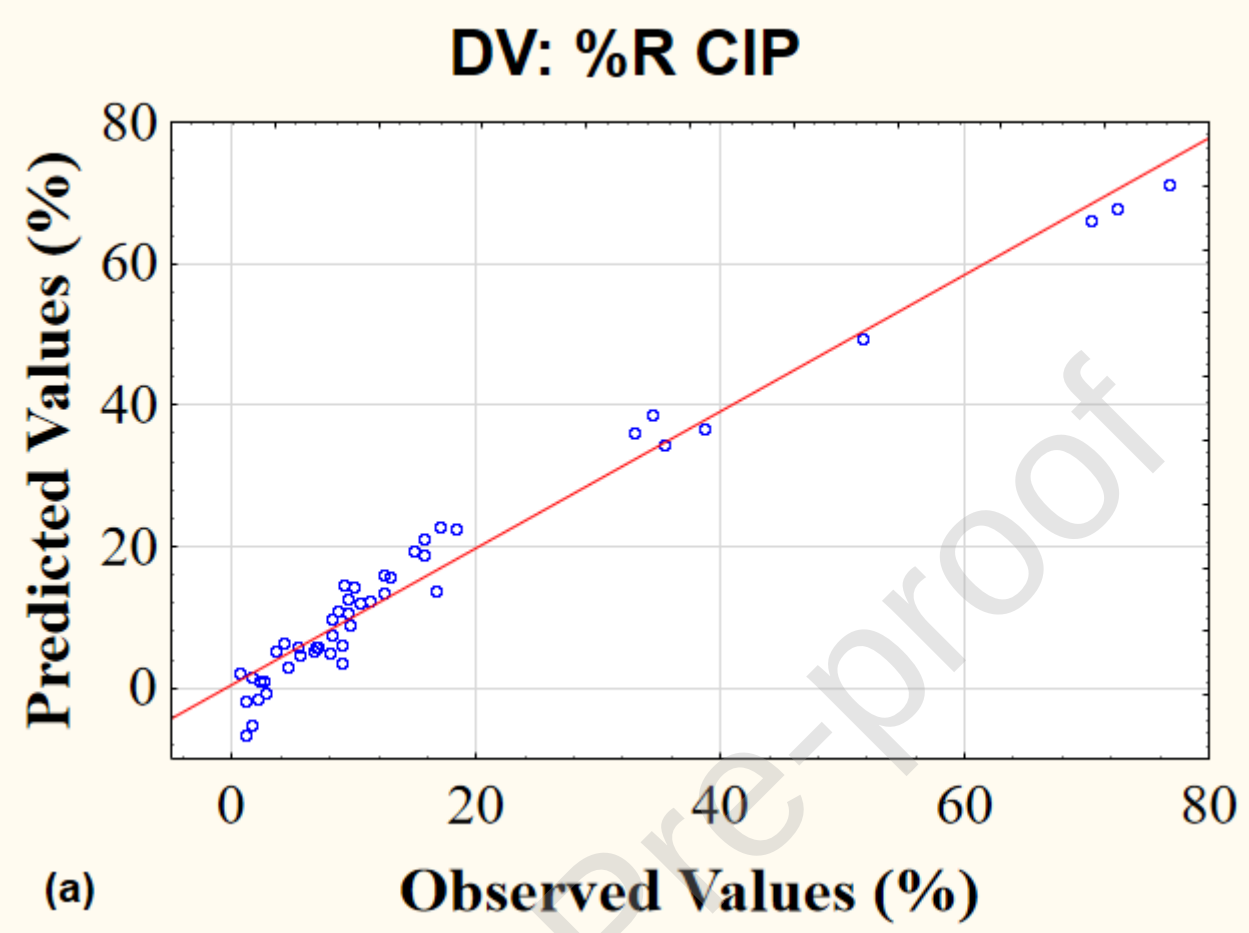

Fig 4b

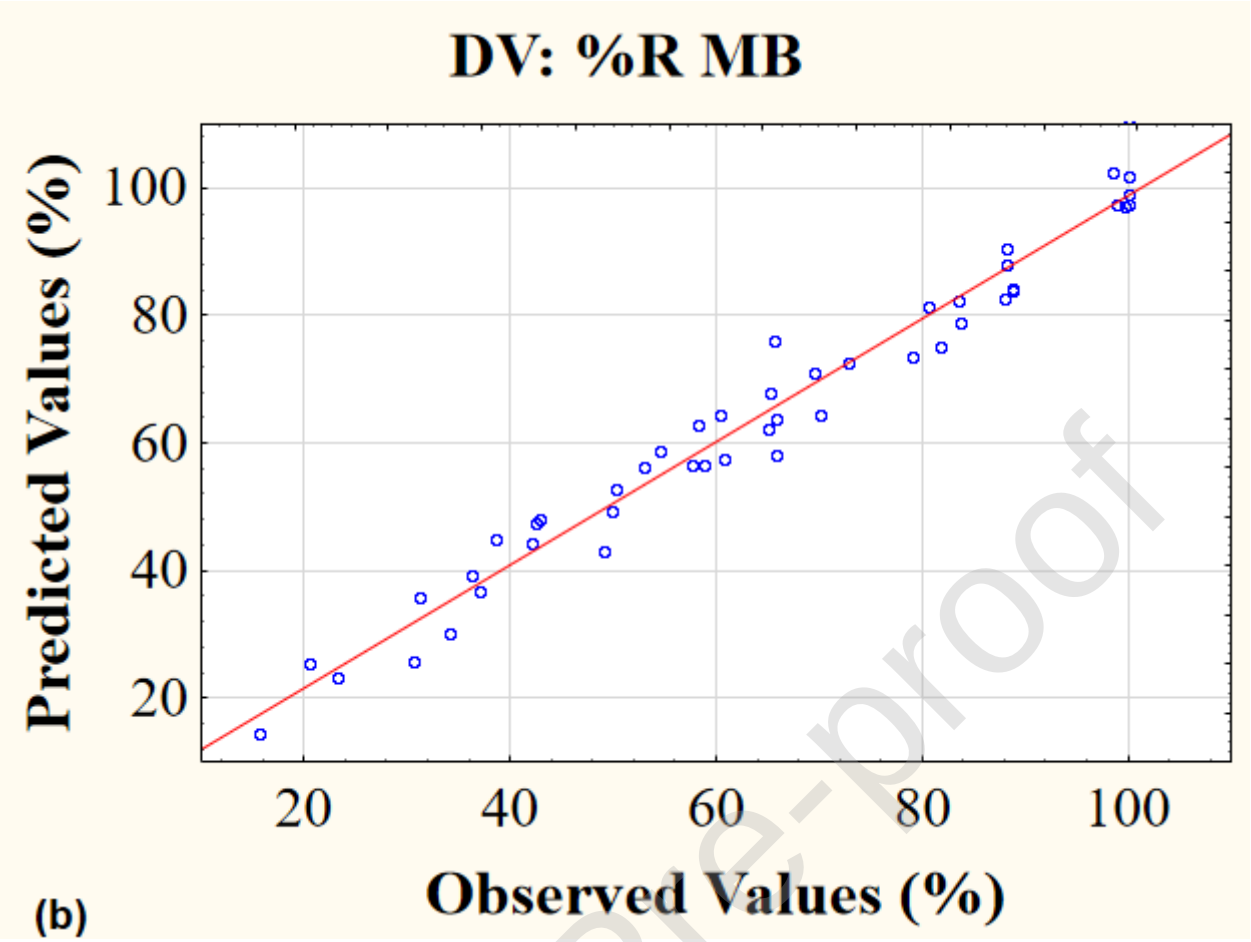

Fig 5a

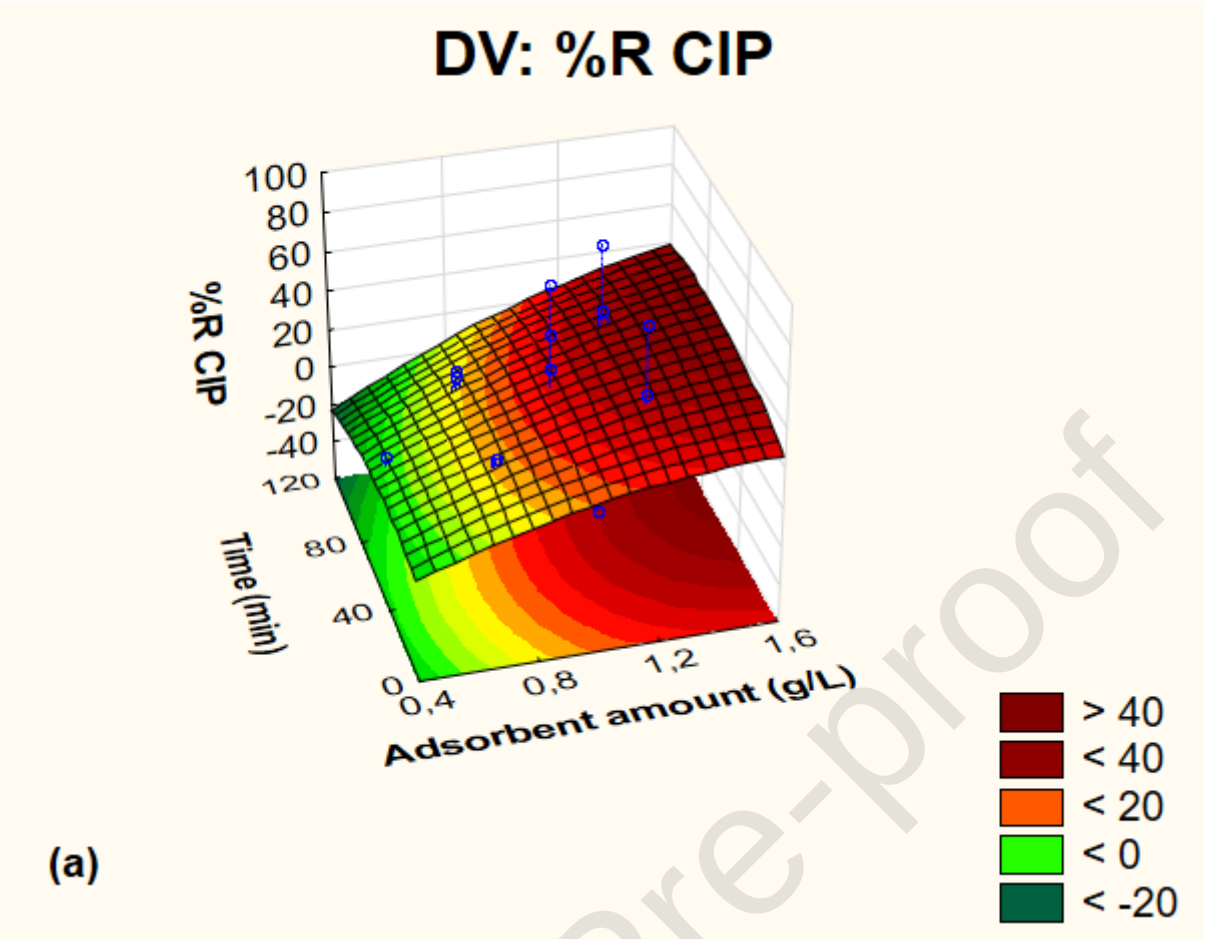

Fig 5b

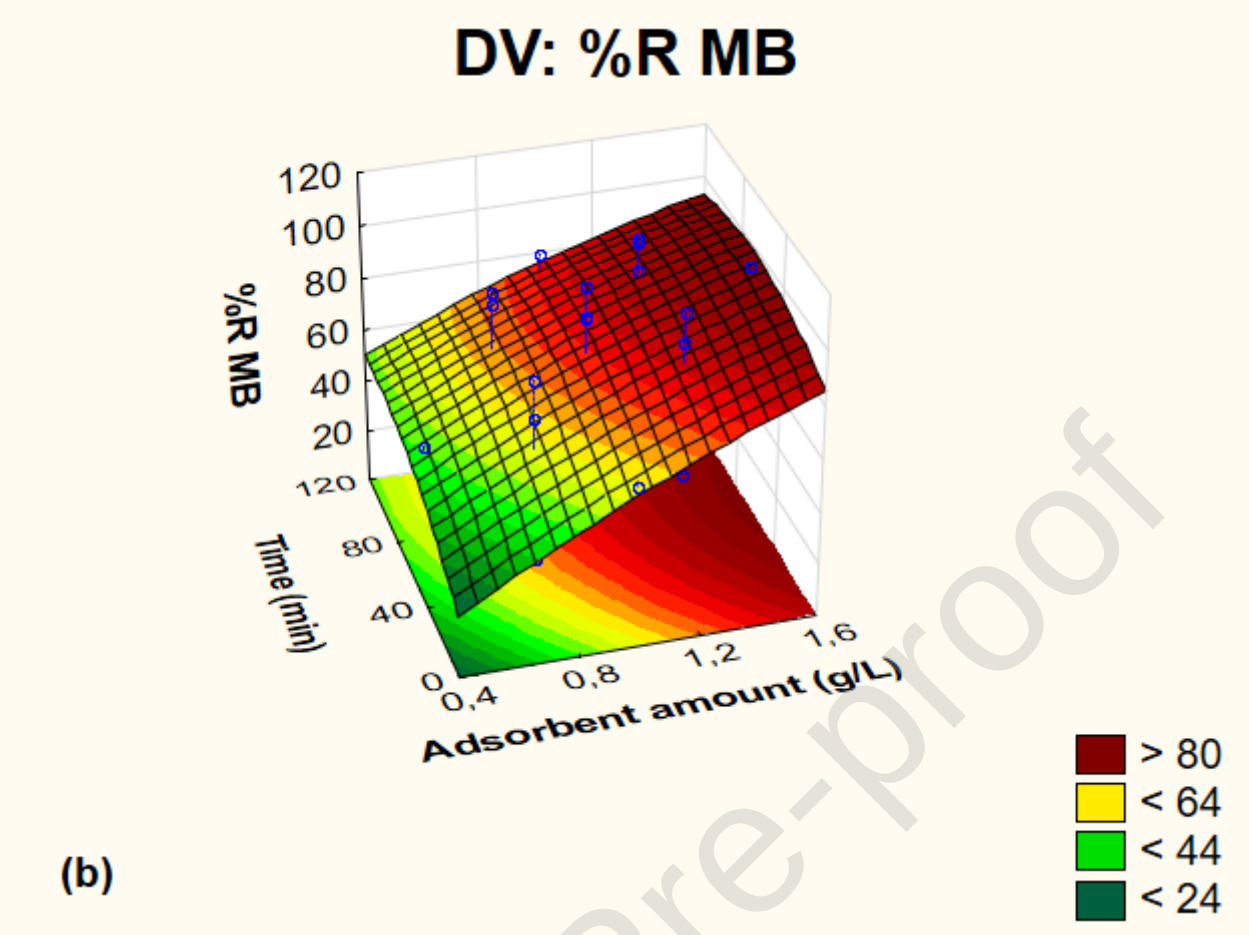

Fig 5c

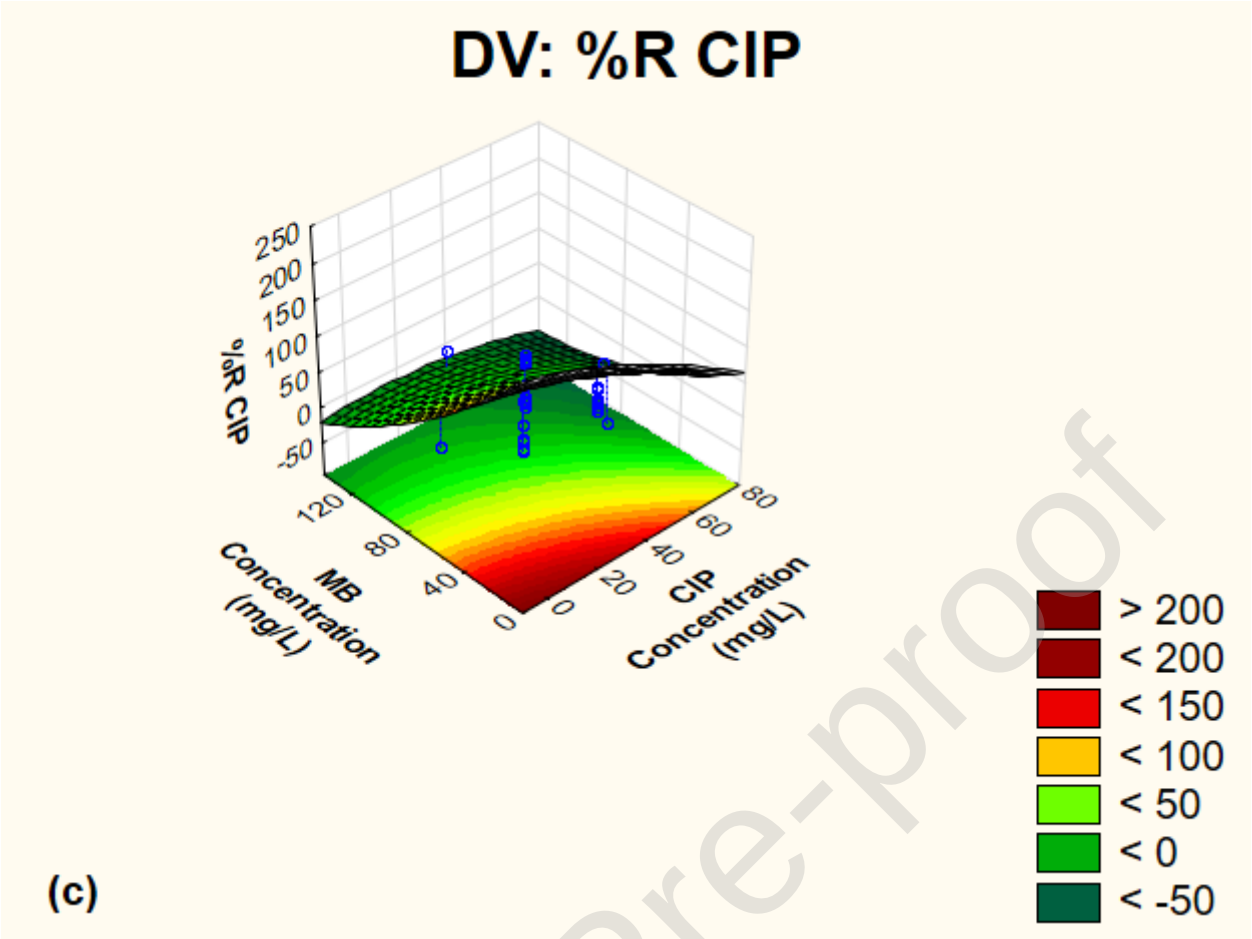

Fig 5d

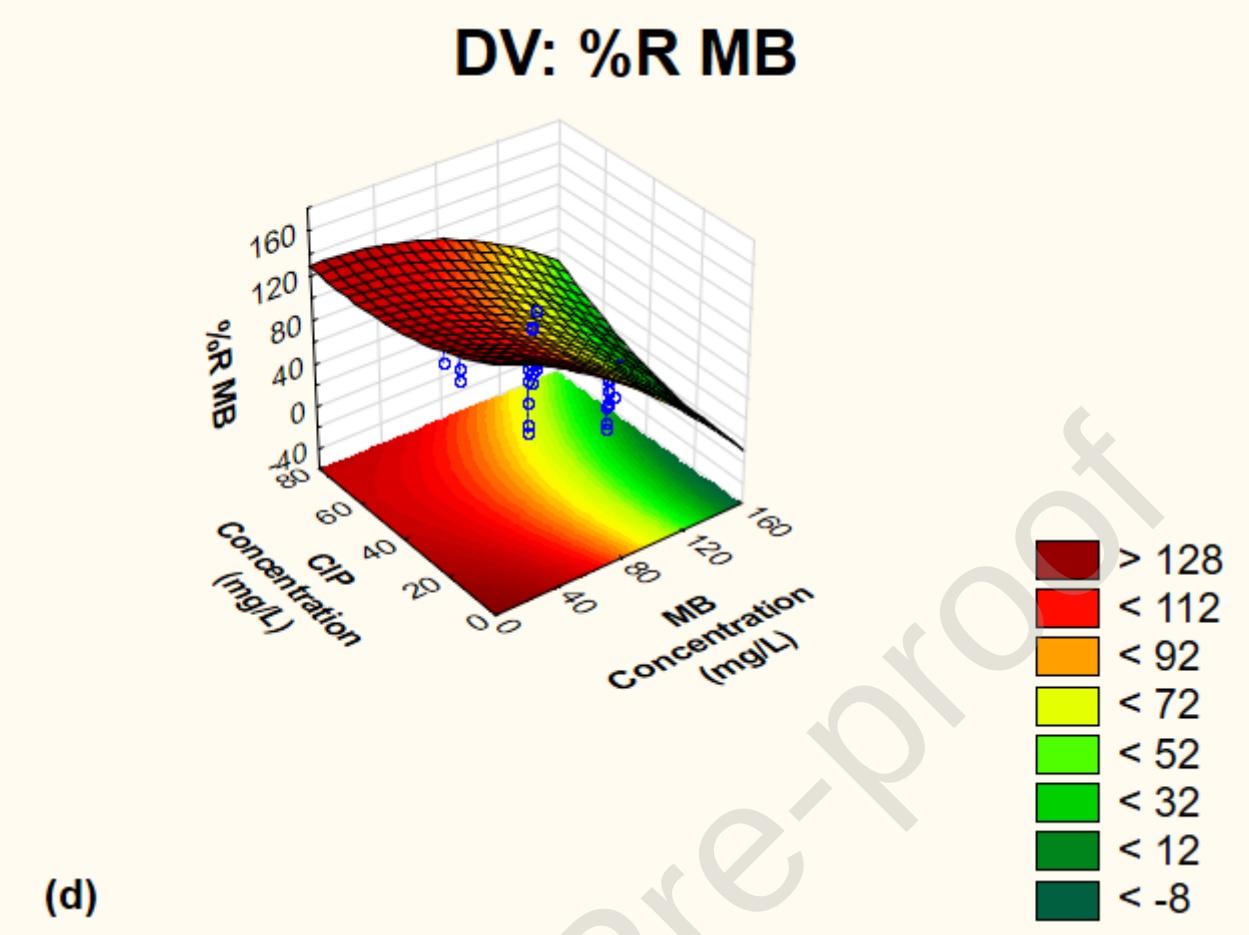

Fig 5e

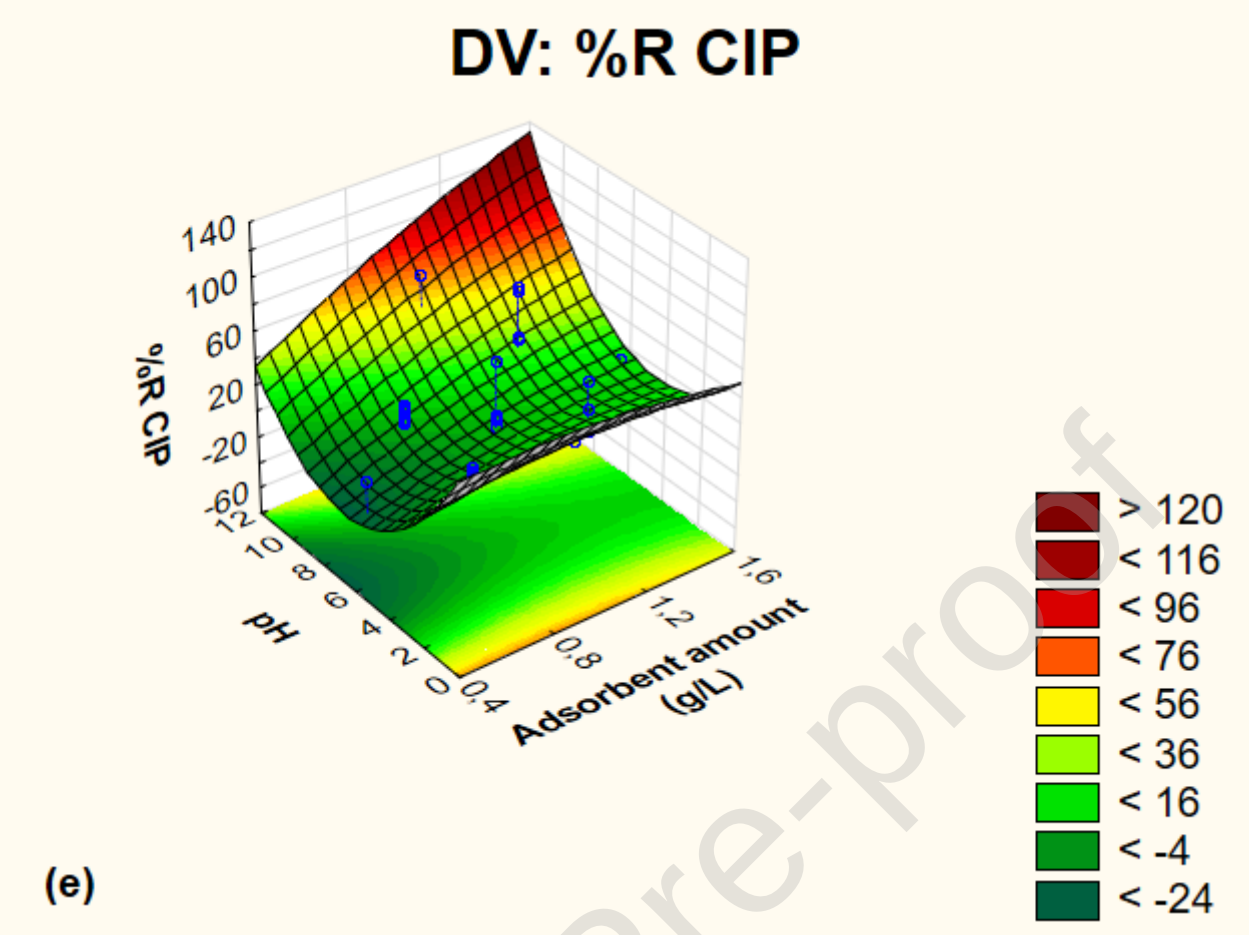

Fig 5f

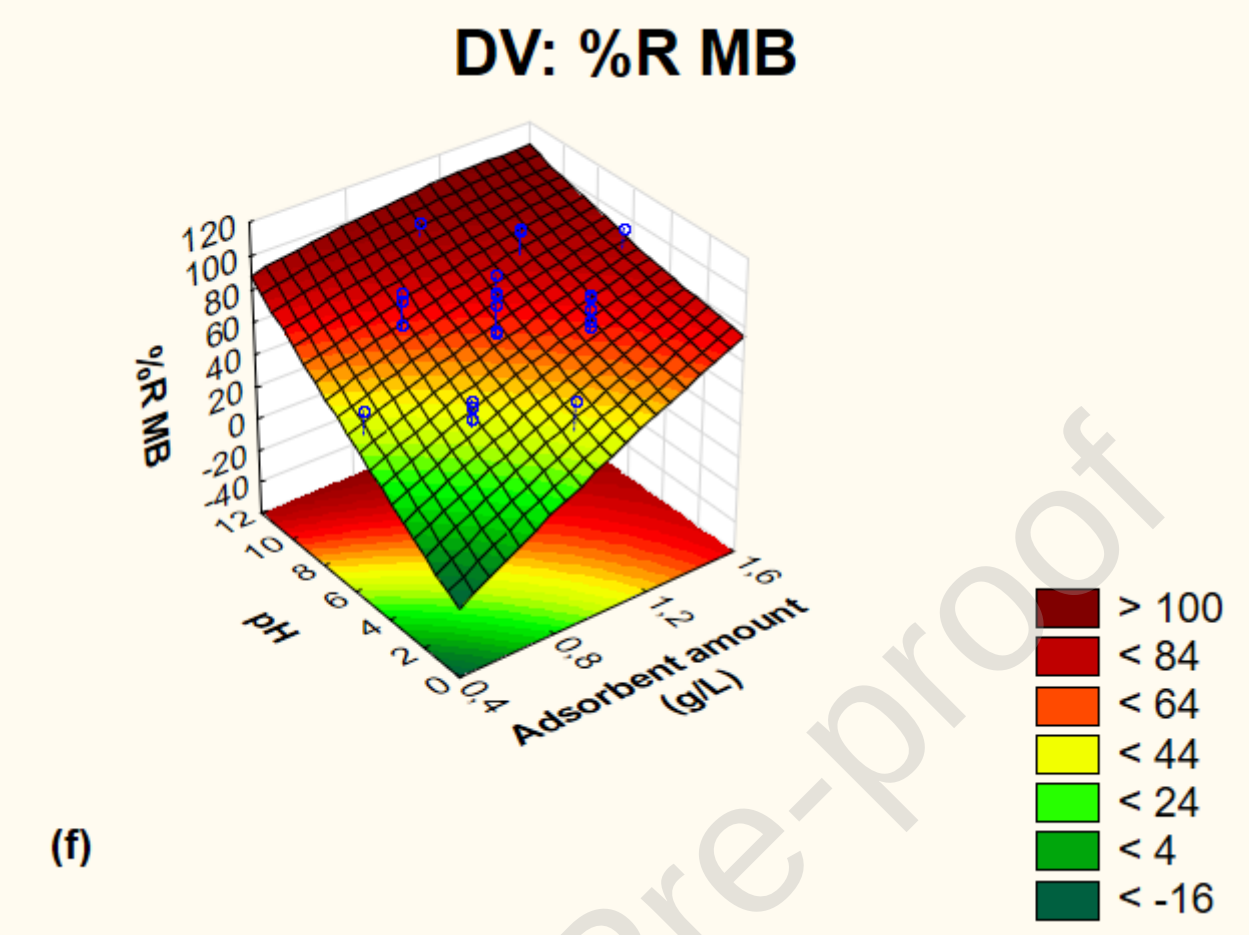

Fig 6

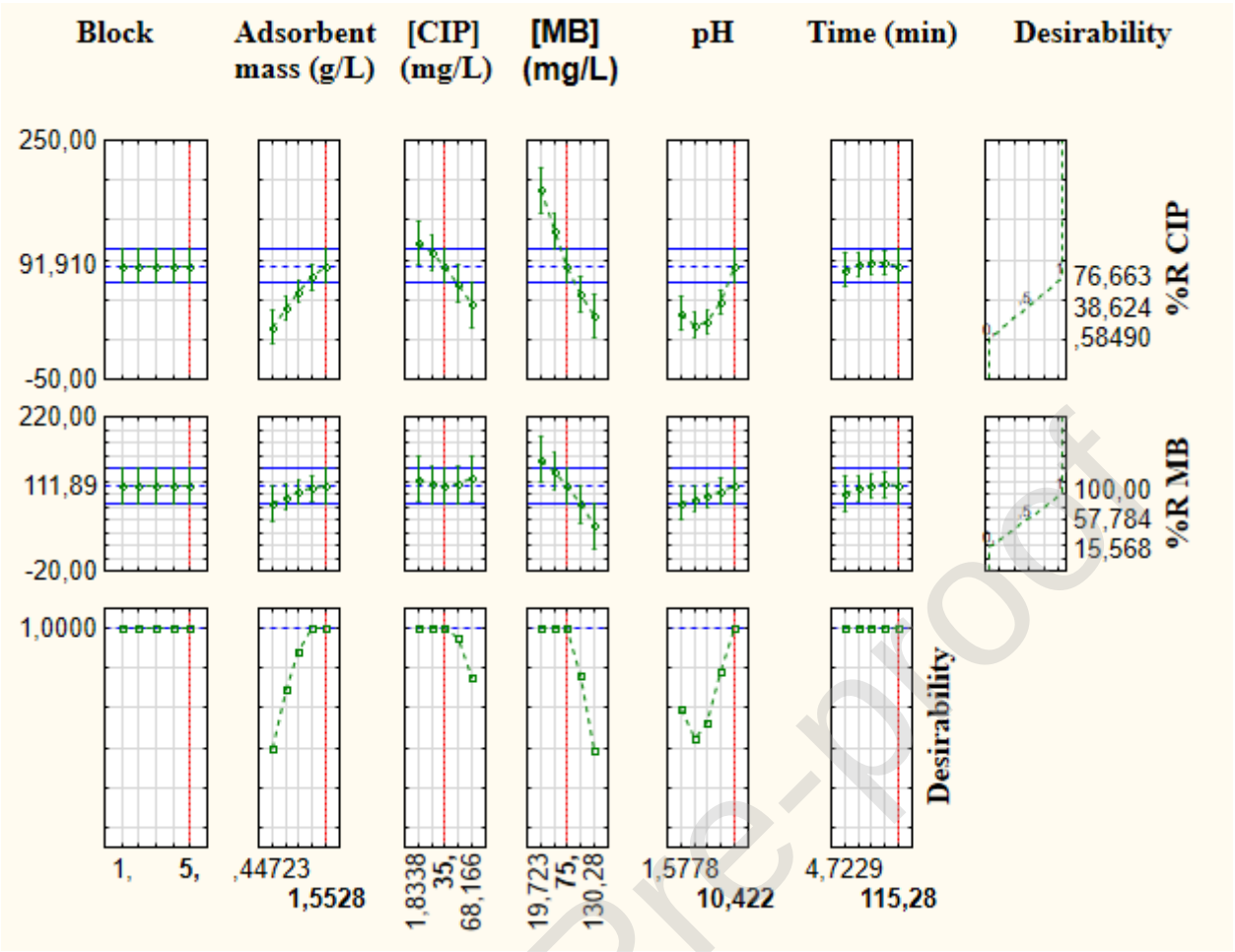

Fig 7

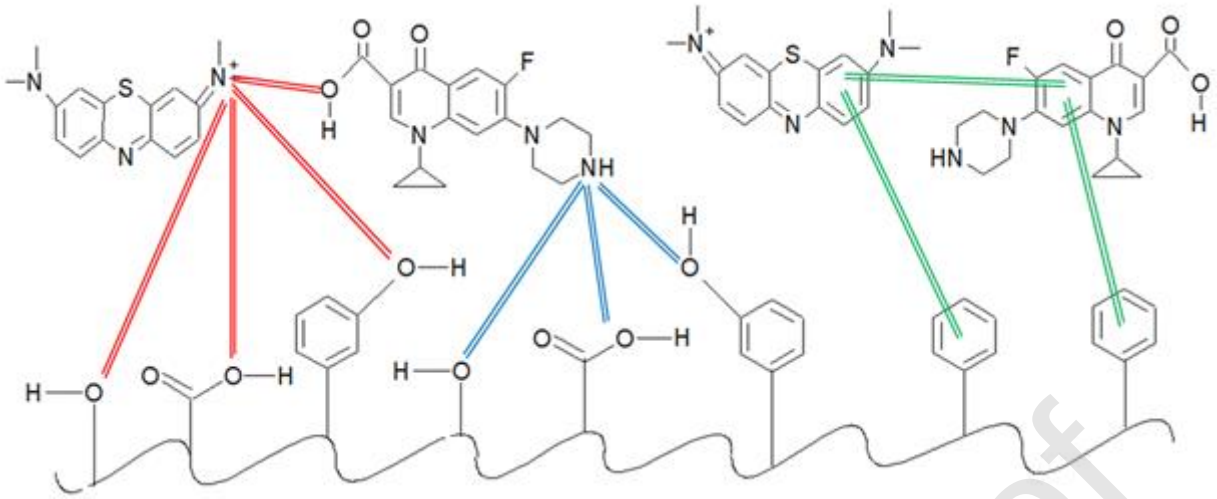

Tables

Table 1. Experimental variables and levels used in the CCD.

Factor code	Factors	Levels				
		-α (-2)	Low (-1)	Central (0)	High (+1)	+α (+2)
X_1	Adsorbent mass (g/L)	0.45	0.75	1	1.25	1.55
X_2	CIP concentration (mg/L)	1.83	20	35	50	68.17
X_3	MB concentration (mg/L)	19.72	50	75	100	130.28
X_4	pH	1.58	4	6	8	10.42
X_5	Contact time (min)	4.72	35	60	85	115.28

Table 2. Surface area and porosity parameters.

	BET surface area (m^2/g)	The pore diameter (nm)	The total pore volume (mm^3/g)
RR-ChR	8.9 ± 0.1	9.6	21.4
RR-ChR-CIP-MB	2.13 ± 0.01	14.6	7.8

Table 3. Thermal parameters of R, ChR and RR-ChR samples.

Sample	$T_{5\%}$[a] (K)	$T_{10\%}$[b] (K)	Char yield at 1123.15 °K	LOI
R	477.15	520.15	9.01	21.10
ChR	413.15	607.15	13.12	22.75
RR-ChR	520.15	550.15	10.12	21.55

[a] Temperature at which 5 % weight loss was recorded by TGA
[b] Temperature at which 10 % weight loss was recorded by TGA

Table 4. Model summary.

	CIP	MB
R-squared (R^2)	0.9667	0.9675
Adjusted R-squared	0.9304	0.9321
MS Residual	24.1629	39.9119

Table 5. Kinetic parameters given by the various models considered for the adsorption of binary solutions of CIP and MB (X_1 = 1.55 g/L ; X_2 = 35 mg/L ; X_3 = 75 mg/L ; X_4 = 10.42 ; X_5 = 115.28 min ; T = 30 ± 1 °C).

	Parameters	CIP	MB
	$q_{e,exp}$	17.3	47.4
BSf(n,α)	q_e	17.5	47.4
	R^2	**0.9994**	**1**
	X^2	0.01	1.2E-4
	RSS	0.1	9.3E-4
PFO	$q_{e,1}$	16.8	47.3
	R^2	**0.9928**	**0.99998**
	X^2	0.2	36E-4
	RSS	1.8	0.03
PSO	$q_{e,2}$	18.2	47.5
	R^2	**0.9886**	**0.99996**
	X^2	0.3	0.01
	RSS	2.9	0.1
Weibull	$q_{e,W}$	17.0	47.4
	R^2	**0.9936**	**1**
	X^2	0.2	1.9E-4
	RSS	1.5	17E-4
Hill	$q_{e,H}$	17.2	47.4
	R^2	**0.9981**	**1**
	X^2	0.04	1.0E-4
	RSS	0.4431	9.3E-4
Brouers–Gaspard	$q_{e,BG}$	17.1	47.4
	R^2	**0.9967**	**1**
	X^2	0.1	1.1E-4
	RSS	0.7	9.97E-4

Table 6. Adsorption isotherm parameters given by the various models considered for the fitting of isotherm data of binary solutions of CIP and MB (X_1 = 1.55 g/L ; X_2 = 35 mg/L ; X_3 = 75 mg/L ; X_4 = 10.42 ; X_5 = 115.28 min ; T = 30 ± 1 °C).

	Parameters	CIP	MB
	$q_{e,exp}$	31.2	79.9
GBS	$q_{e,max}$	31.8	80.3
	R^2	**0.9639**	**0.9638**
	X^2	4.7	23.1
	RSS	9.5	46.3
BS	$q_{e,maxBS}$	32.8	84.5
	R^2	**0.9665**	**0.9723**
	X^2	4.4	17.7
	RSS	13.2	53.2
Freundlich	K_F	6.5	52.0
	R^2	**0.9089**	**0.9169**
	X^2	11.9	53.2
	RSS	47.8	212.8
Jovanovich	$q_{e,maxJ}$	34.3	72.0
	R^2	**0.9711**	**0.6032**
	X^2	3.8	254.3
	RSS	15.1	1017.3
HS sips	$q_{e,maxHS}$	38.2	97.9
	R^2	**0.9527**	**0.9697**
	X^2	6.2	19.4
	RSS	18.6	58.1
Langmuir	$q_{e,maxL}$	45.7	70.1
	R^2	**0.9586**	**0.8236**
	X^2	5.4	113.1
	RSS	21.8	452.2
BG isotherm	$q_{e,maxBG}$	35.3	91.2
	R^2	**0.9578**	**0.9706**
	X^2	5.5	18.8
	RSS	16.6	56.5
DR isotherm	$q_{e,maxDR}$	22.0	67.7
	K_{DR}	3E-07	1E-08
	E	1.3	7.1
	R^2	**0.8292**	**0.9378**
	X^2	3.9	19.3

Table 7. Literature comparison of CIP and MB adsorption capacities for different materials.

CIP Removal			MB removal		
Adsorbent	Adsorption capacity (mg/g)	References	Adsorbent	Adsorption capacity (mg/g)	References
Aluminum hydrous oxide	14.7	[1]	H_2O_2-treated rice husk	18.7	[2]
Kaolinite	7.0	[3]	Physical/O3+Steam treated Rice husk	27.8	[4]
Aluminum-pillared clays	17.8	[5]	Agave americana fibers	44.3	[6]
Iron hydrous oxide	25.8	[1]	Cotton stalk	4.5–15.7	[7]
RR-ChR biocomposite	17.3	This work	RR-ChR biocomposite	47.4	This work

Table 8. Thermodynamic parameters for the adsorption of binary solutions of CIP and MB onto RR-ChR at different temperatures (X_1 = 1.55 g/L ; X_2 = 35 mg/L ; X_3 = 75 mg/L ; X_4 = 10.42 ; X_5 = 115.28 min).

Contaminant	T (°K)	K_d	ΔH^0 (kJ/mol)	ΔS^0 (J/mol.K)	ΔG^0 (kJ/mol)	ΔG^0_{cal} (kJ/mol)
CIP	293.15	2.05	46.01	163.38	-1.77	-1.76
	303.15	4.24			-3.40	-3.64
	313.15	7.61			-5.03	-5.28
	323.15	11.83			-6.66	-6.63
MB	293.15	98.91	37.59	165.47	-10.77	-11.19
	303.15	119.42			-12.42	-12.05
	313.15	247.49			-14.07	-14.34
	323.15	383.37			-15.72	-15.98

References

[1] K.G. Karthikeyan, Sorption of the Antimicrobial Ciprofloxacin To Aluminum and Iron Hydrous Oxides, 39 (2005) 9166–9173.

[2] P.M.K. Reddy, S. Mahammadunnisa, Low-cost adsorbents from bio-waste for the removal of dyes from aqueous solution, (2013) 4111–4124. doi:10.1007/s11356-012-1360-8.

[3] Z. Li, H. Hong, L. Liao, C.J. Ackley, L.A. Schulz, R.A. Macdonald, A.L. Mihelich, S.M. Emard, Colloids and Surfaces B : Biointerfaces A mechanistic study of ciprofloxacin removal by kaolinite, Colloids Surfaces B Biointerfaces. 88 (2011) 339–344. doi:10.1016/j.colsurfb.2011.07.011.

[4] P.M. Kumar, R.K. Krushnamurty, Preparation of activated carbons from bio-waste : effect of surface functional groups on methylene blue adsorption, (2014). doi:10.1007/s13762-014-0506-2.

[5] M.E.R. Jalil, M. Baschini, K. Sapag, Removal of ciprofloxacin from aqueous solutions using pillared clays, Materials (Basel). 10 (2017) 17–19. doi:10.3390/ma10121345.

[6] A.M. Ben Hamissa, F. Brouers, M.C. Ncibi, M. Seffen, Kinetic Modeling Study on Methylene Blue Sorption onto Agave americana fibers: Fractal Kinetics and Regeneration Studies, Sep. Sci. Technol. 48 (2013) 2834–2842. doi:10.1080/01496395.2013.809104.

[7] B. Acemio, M.H. Alma, M. Usta, Removal of methylene blue from aqueous solution using cotton stalk , cotton waste and cotton dust Murat Ertas, 183 (2010) 421–427. doi:10.1016/j.jhazmat.2010.07.041.